JCB Journal of Cell Biology

ARTICLE

Treacle and TOPBP1 control replication stress response in the nucleolus

Artem K. Velichko[1,2,3], Natalia Ovsyannikova[4], Nadezhda V. Petrova[1], Artem V. Luzhin[1,2], Maria Vorobjeva[1], Alexey S. Gavrikov[5], Alexander S. Mishin[5], Igor I. Kireev[4,6], Sergey V. Razin[1], and Omar L. Kantidze[1]

Replication stress is one of the main sources of genome instability. Although the replication stress response in eukaryotic cells has been extensively studied, almost nothing is known about the replication stress response in nucleoli. Here, we demonstrate that initial replication stress–response factors, such as RPA, TOPBP1, and ATR, are recruited inside the nucleolus in response to drug-induced replication stress. The role of TOPBP1 goes beyond the typical replication stress response; it interacts with the low-complexity nucleolar protein Treacle (also referred to as TCOF1) and forms large Treacle–TOPBP1 foci inside the nucleolus. In response to replication stress, Treacle and TOPBP1 facilitate ATR signaling at stalled replication forks, reinforce ATR-mediated checkpoint activation inside the nucleolus, and promote the recruitment of downstream replication stress response proteins inside the nucleolus without forming nucleolar caps. Characterization of the Treacle–TOPBP1 interaction mode leads us to propose that these factors can form a molecular platform for efficient stress response in the nucleolus.

Introduction

DNA replication stress refers to the slowing or stalling of replication fork progression and downstream events such as replication fork reversal or collapse. Replication stress induced by intrinsic and extrinsic factors is a major source of genome instability in eukaryotes. Several interconnected DNA damage response (DDR) pathways maintain genome stability under replication stress conditions. In most cases, replication stress–associated DDR begins with the activation of the ATR-CHK1 axis to provide transient proliferation arrest, stabilize the stalled forks, and prevent dormant origin firing. Stretches of single-stranded DNA accumulated as a result of replication fork stalling are bound by replication protein A (RPA) and serve as a platform for the recruitment of ATR-activating factors (Blackford and Jackson, 2017). Those factors include ATR-interacting protein (ATRIP), 9-1-1 complex (RAD9-RAD1-HUS1), topoisomerase II binding protein 1 (TOPBP1), and Ewing tumor-associated antigen 1 (ETAA1; Lee et al., 2016; Zou, 2017). Activated ATR phosphorylates several downstream targets, including its main effector kinase CHK1. The only known role for TOPBP1 in the replication stress response is to activate ATR through its ATR-activation domain (AAD; Wardlaw et al., 2014). However, the presence of nine BRCT domains grouped in various configurations makes TOPBP1 an ideal platform for multifaceted protein–protein interactions. Two other DDR pathways involved in fork stabilization and recovery are Fanconi anemia repair and the Rad51-BRCA branch of homologous recombination repair (Berti et al., 2020).

Nucleoli, the sites of ribosome biogenesis, are formed around arrays of ribosomal gene repeats (rDNA), which are transcribed by RNA polymerase I (Pol I) to produce pre-rRNA (Cerqueira and Lemos, 2019). In the nucleolus, RNAs and hundreds of different proteins are segregated into three major types of immiscible liquid phases: fibrillar centers (FCs) containing active Pol I machinery, the dense fibrillar component enriched in the fibrillarin protein, and the granular component enriched in the nucleophosmin (NPM1/B23; Feric et al., 2016; Yao et al., 2019). The immiscibility of nucleolar subcompartments imposes certain constraints on specific molecular processes. Indeed, many DNA repair factors are normally excluded from nucleoli because they are thought to be incompatible with nucleolar liquid phases (van Sluis and McStay, 2019). In response to rDNA-specific double-stranded breaks (DSBs), FCs migrate to the nucleolar periphery and form so-called nucleolar caps that enable the recruitment of repair factors and facilitate DSB repair (van Sluis and McStay, 2019). Here, we questioned how the DNA replication stress response proceeds in the nucleolus.

[1]Institute of Gene Biology Russian Academy of Sciences, Moscow, Russia; [2]Center for Precision Genome Editing and Genetic Technologies for Biomedicine, Institute of Gene Biology Russian Academy of Sciences, Moscow, Russia; [3]Institute for Translational Medicine and Biotechnology, Sechenov First Moscow State Medical University, Moscow, Russia; [4]A.N. Belozersky Institute of Physico-Chemical Biology, Lomonosov Moscow State University, Moscow, Russia; [5]Shemyakin–Ovchinnikov Institute of Bioorganic Chemistry Russian Academy of Sciences, Moscow, Russia; [6]V.I. Kulakov National Medical Research Center for Obstetrics, Gynecology, and Perinatology, Moscow, Russia.

Correspondence to Omar L. Kantidze: kantidze@gmail.com; Sergey V. Razin: sergey.v.razin@usa.net.

We investigated the molecular mechanisms involved in protecting the cell from replication stress induced in rDNA (nucleolus) of the higher eukaryotes. Although the nucleolar replication stress response shares many features with the classic response operating elsewhere in the genome, it also exhibits some unique characteristics, the most important being its dependence on nucleolar protein Treacle and the formation of large Treacle–TOPBP1 foci. Our data show the importance of macromolecular assembly of Treacle and TOPBP1 as a scaffolding platform, which provides recruitment of stress response factors inside the nucleoli and reinforces ATR activation under DNA replication stress, thus limiting genome instability.

Results

Replication stress response induced in nucleoli

Although the replication stress response in eukaryotic cells has been extensively studied, almost nothing is known about the response in nucleoli. However, because it is a phase-separated, membraneless compartment, the nucleolus can represent an obstacle for some proteins involved in the typical replication stress response (van Sluis and McStay, 2019). Nucleolar proteome studies have revealed that TOPBP1, ATR, and ATRIP are present in the nucleoli of cancer cells (Andersen et al., 2005; Couté et al., 2006), an observation that might reflect elevated levels of DNA replication stress in these cells. Indeed, using immunofluorescence analysis, we observed nucleolar TOPBP1 foci in approximately half of nontreated S phase HeLa cells (Fig. 1, A and B). Precise analysis of S phase HeLa cells demonstrated that the nucleolar TOPBP1 foci persisted in the cells during early and mid-S phase, when the replication of ribosomal genes takes place (Fig. S1 A). To verify further that the nucleolar TOPBP1 foci arise in response to DNA replication stress, we immunostained TOPBP1 in HeLa cells treated with hydroxyurea (HU) or aphidicolin (APH). In both cases, the number of cells containing nucleolar TOPBP1 foci began to increase after a 6-h incubation in culture medium supplemented with the drugs and reached a maximum level after 12 h of drug exposure (Fig. 1 C and Fig. S1 B). To ensure that the observed phenomenon is not limited to HeLa cells, we analyzed several human (U2OS, MCF7, HeLa Kyoto, $p53^{wt}$, and $p35^{ko}$ HCT116) and mouse (CT26) cancer cell lines as well as normal human fibroblasts. In all cases, we found a significant increase in the number of cells possessing nucleolar TOPBP1 foci in response to several hours of APH treatment (Fig. S1 C). It should be noted that the treatment of the cells with APH or HU induced TOPBP1 foci formation not only in nucleoli but also in the nucleoplasm (i.e., at the genomic sites outside the rDNA), as evidenced by the overexposed images obtained using structured illumination microscopy (SIM; Fig. S1 D).

Cell-cycle profiling revealed that this 12-h incubation of HeLa cells with APH or HU accumulated most of the cells in the S phase (Fig. S2 A). To rule out the possibility that the increase of nucleolar TOPBP1 foci-possessing cells in the population was caused by the synchronization of the cells in the S phase, we synchronized HeLa cells in the S phase and then treated them with APH for different periods (1–12 h; Fig. S2 B). In this experiment, we could not use a widely accepted double-thymidine synchronization method because the method induced replication stress itself; thus, we synchronized the cells using nocodazole at the G2/M phase border and released them for 9 h to accumulate in the S phase. This experiment clearly showed that the mere accumulation of the cells in the S phase did not result in nucleolar TOPBP1 foci formation (control in Fig. S2 B). These foci were induced only in response to prolonged replication stress (Fig. S2 B).

To determine whether TOPBP1 is enriched at the ribosomal genes, we performed chromatin immunoprecipitation (ChIP) with the corresponding antibody. In HeLa cells treated with APH for 12 h, TOPBP1 was highly enriched at the 45S RNA coding sequences, with two peaks corresponding to the 45S RNA transcription start site and the 28S RNA coding region (Fig. 1 D). Combined TOPBP1 immunostaining and FISH for rDNA repeats corroborated these results; large nucleolar TOPBP1 foci were covered with dot-like rDNA FISH signals (Fig. 1 E).

SIM studies revealed that in most APH-treated HeLa cells, TOPBP1 formed one large focus inside the nucleolus (Fig. 1 F) that corresponded to the large FC, as evidenced by colocalization with Pol I or with its transcription factor UBF (Fig. 1 G). To gain more insight into the structure of nucleolar TOPBP1 foci, we applied stochastic optical reconstruction microscopy (STORM). We found that nucleolar TOPBP1 foci are spherical sponge-like structures, which potentially refers to their "semifluid" nature (Fig. 1 H).

In APH-treated HeLa cells, replicating DNA (marked with 5-ethynyl-2′-deoxyuridine [EdU] incorporation) and major replication stress response factors (RPA, ATR, and CHK1) occupied the periphery of the TOPBP1-positive large FCs, thus mimicking the distribution of FISH-marked rDNA repeats (Fig. 2 A). Results of ChIP-quantitative PCR (qPCR) analyses also showed partial coincidence of replication stress–induced TOPBP1 and RPA (Fig. 2 B). Indirect immunofluorescence and ChIP-qPCR demonstrated that histone H2AX was extensively phosphorylated at sites of rDNA repeats in response to prolonged replication stress (Fig. 3, A and B). Since TOPBP1 and γH2AX accumulation in nucleoli might be linked to the stabilization of R loops and/or DSB formation (Mooser et al., 2020; Velichko et al., 2019), we further elucidated these possibilities. First, using overexpression of RNase H, which specifically degrades RNA in R loops, we demonstrated that replication stress–induced nucleolar TOPBP1 foci did not depend on R loop stabilization (Fig. 3 C). Second, we showed that 12 h of APH or HU treatment did not induce DSBs (Fig. 3, D and E). Given its importance, we checked this result using the neutral comet assay (Fig. 3 D) as well as a much more specific approach—terminal deoxynucleotidyl transferase (TdT)–mediated labeling of DSBs followed by biotin-streptavidin precipitation and qPCR analysis of the precipitated DNA (DSB detection assay; Fig. 3 E; Ju et al., 2006; Ray et al., 2013). The latter method allowed us to analyze DSBs arising specifically in rDNA. It should be emphasized that both methods were sensitive enough to detect a small number of DSBs introduced into rDNA by homing endonuclease I-PpoI.

We next investigated whether replication stress–induced TOPBP1 accumulation in the nucleoli depends on ATR. Indirect immunofluorescence and ChIP-qPCR analyses of cells genetically depleted of ATR clearly demonstrated its necessity for the formation of large nucleolar TOPBP1 foci in response to APH treatment (Fig. 2, C and D). These data were confirmed by using

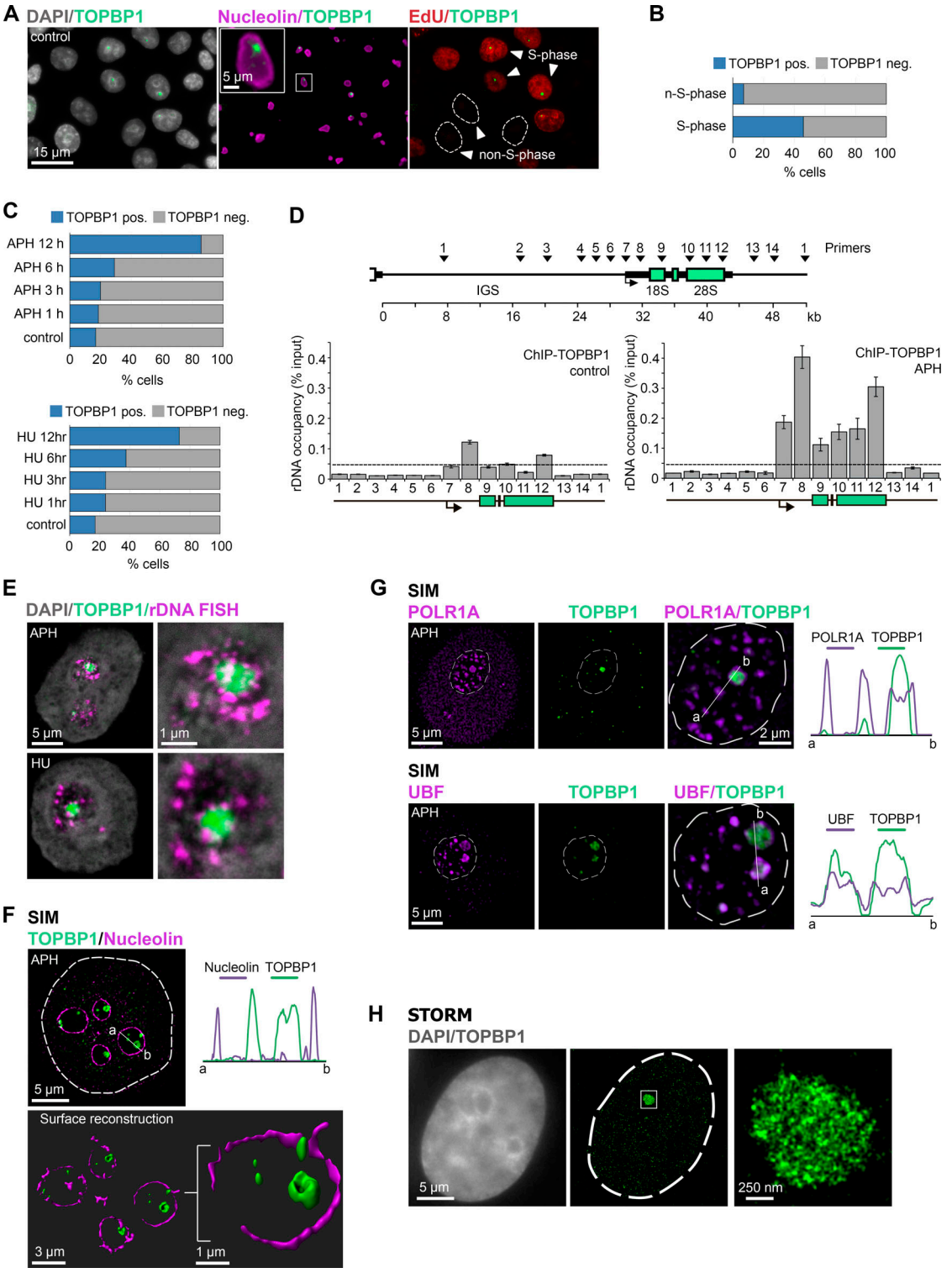

Figure 1. **Replication stress induces the accumulation of TOPBP1 in nucleoli. (A)** Asynchronous HeLa cells were pulse labeled with EdU (10 µM, 30 min) and immunostained for TOPBP1 (green) and nucleolin (magenta). EdU (red) was revealed by click chemistry. The DNA was stained with DAPI (gray). S phase and non–S phase cells are shown by white arrows. **(B)** Quantification of cells presented in A. Percentage of cells containing large TOPBP1 foci among S phase and non–S phase cells is shown. **(C)** HeLa cells were treated with APH (1 µM) or HU (1 mM) for 1, 3, 6, or 12 h and immunostained for TOPBP1. Control represents untreated cells. Percentage of cells containing large TOPBP1 foci is shown. **(D)** Occupancy of TOPBP1 at rDNA in control (untreated) and APH-treated (1 µM, 12 h) HeLa cells. ChIP with IgG and antibody against TOPBP1 was followed by qPCR using the rDNA amplicons positioned as indicated on the scheme above (numbered arrowheads). Data are represented relative to the input. Values are the mean ± SD from at least three independent replicates. IGS, intergenic spacer. **(E)** Representative images of rDNA repeats (magenta) revealed by FISH along with immunostained TOPBP1 (green) in HeLa cells treated either with APH (1 µM) or with HU (1 mM) for 12 h. **(F)** APH-treated (1 µM, 12 h) HeLa cells were stained for TOPBP1 (green) and nucleolin (magenta) and analyzed by SIM. The nucleus is marked by a dashed line. Colocalization analysis was performed on the merged images. Graphs illustrate quantification in

arbitrary units of the distribution of TOPBP1 and nucleolin fluorescence along the lines shown in the figure. **(G)** APH-treated (1 µM, 12 h) HeLa cells were stained for TOPBP1 (green) and either Pol I (POLR1) or UBF (magenta) and analyzed by SIM. Nucleoli are marked by dashed lines. Colocalization analysis was performed on the merged images. Graphs illustrate quantification in arbitrary units of the distribution of TOPBP1 and corresponding nucleolar protein fluorescence along the lines shown in the figures. **(H)** Representative STORM image of TOPBP1 (green) in human HeLa cells that had been treated with APH (1 µM, 12 h), fixed, and immunostained for TOPBP1. The DNA was stained with DAPI (gray). neg., negative; pos., positive.

the pharmacological inhibitor of ATR (Fig. 2 C). Bearing in mind that ATR has two known activators, TOPBP1 and ETAA1, we investigated the contribution of ETAA1 to the nucleolar replication stress response. We found that following prolonged replication stress, ETAA1 is neither localized in the nucleoli (Fig. S2 C) nor involved in the accumulation of TOPBP1 in nucleoli (Fig. 2 C). The latter is evidenced by TOPBP1 immunostaining of ETAA1 knockdown HeLa cells treated with APH (Fig. 2 C). In summary, these data reveal that the replication stress response in nucleoli is only induced as a result of prolonged treatment of the cells with APH or HU and suggest that TOPBP1 plays an important architectural and signaling role in the nucleolar replication stress response.

Replication stress stimulates TOPBP1–Treacle interaction

Recently, we and others have found that the nucleolar protein Treacle is indispensable for recruitment and/or retention of TOPBP1 in nucleoli in response to DNA damage (Mooser et al., 2020; Velichko et al., 2019). Here, we analyzed whether Treacle is involved in the replication stress response that takes place in nucleoli. Indirect immunofluorescence and ChIP-qPCR studies with HeLa cells depleted of Treacle demonstrated the necessity of replication stress–induced recruitment of TOPBP1 to ribosomal genes and the formation of large TOPBP1-positive FCs (Fig. 4, A–C). Protein coimmunoprecipitation analysis clearly showed that in HeLa cells treated with APH or HU, Treacle and TOPBP1 physically interact with each other (Fig. 4 D). Replication stress made Treacle and TOPBP1 more resistant to high-salt extraction, as evidenced by Western blot analysis of the chromatin fraction extracted with increasing NaCl concentrations (Fig. 4 E). The mobility of Treacle-GFP localized in TOPBP1-positive large FCs significantly decreased in response to replication stress, as measured by FRAP (Fig. 4 F). To gain more insight into the mutual spatial arrangement of Treacle and TOPBP1, we applied indirect immunofluorescence followed by double-STORM analysis (Fig. 4 G). We found that within replication stress–induced large FCs, both Treacle and TOPBP1 formed sponge-like structures that were highly intermingled (Fig. 4 G). Together, these results reveal that upon replication stress, Treacle (i) interacts with TOPBP1, stimulating its accumulation in large FCs, and (ii) becomes strongly associated (along with TOPBP1) with the insoluble nuclear fractions. Taking into account that TOPBP1 can form phase-separated condensates (Frattini et al., 2021), the observed TOPBP1–Treacle macromolecular assemblies resistant to salt extraction may represent nucleoli-specific scaffolds for efficient replication stress response. To study this issue further, we next analyzed the TOPBP1–Treacle interaction in greater detail.

Characterization of TOPBP1–Treacle interaction

TOPBP1 is a modular protein consisting of the AAD and nine BRCT domains (0–8), which are present in single (BRCT3 and 6) or clustered (BRCT0–2, 4–5, and 7–8) configurations (Fig. 5 A). An interaction mode of TOPBP1 with Treacle is still far from being completely understood. It has only been demonstrated, using the protein coimmunoprecipitation approach, that mutations in BRCT1, 2, and 5 strongly affect the ability of TOPBP1 to bind Treacle (Mooser et al., 2020). We decided to further study the TOPBP1–Treacle interaction and its impact on ATR activation in nucleoli and its repression of nucleolar transcription using FLAG-tagged deletion mutants of TOPBP1 lacking individual domains (Wang et al., 2011). These proteins were transiently expressed in HeLa cells and revealed by the anti-FLAG antibody along with endogenous Treacle or incorporated 5-ethynyl uridine (EU) to measure the level of nucleolar transcription. As Sokka et al. (2015) reported, the overexpression of full-sized TOPBP1 led to the formation of numerous large foci of TOPBP1, which were located on the periphery of the nucleoli and in the nucleoplasm (Fig. 5 B). These foci also contained Treacle, regardless of their location relative to nucleoli (Fig. 5 B). The formation of the FLAG-TOPBP1 foci was strongly dependent on Treacle, as evidenced by studies of cells depleted of Treacle (Fig. 5 C). Protein coimmunoprecipitation analysis demonstrated the existence of the physical interaction of FLAG-TOPBP1 and Treacle (Fig. 5 D). Moreover, FLAG-TOPBP1 was enriched at the 45S RNA coding sequences, as demonstrated by ChIP-qPCR (Fig. 5 E).

Analysis of the deletion mutants suggested that BRCT5 and AAD are indispensable for nucleolar localization (Fig. 5, F and G), efficient activation of ATR (Fig. 5 H), and nucleolar transcription silencing (Fig. 5 I and Fig. S3). Notably, the distribution of TOPBP1 lacking AAD was the same as full-length FLAG-TOPBP1 in the cells depleted for either ATR or Treacle (Fig. 5, F and G). This observation may reflect the fact that ATR activation is a prerequisite for TOPBP1 binding to Treacle. The deletion of TOPBP1 BRCT1 or 2 partially compromised ATR activation and nucleolar transcription silencing (Fig. 5, H and I), agreeing well with recently published data showing the role of these BRCT domains in TOPBP1–Treacle interaction (Mooser et al., 2020). Interestingly, the deletion of TOPBP1 BRCT7 or 8 did not affect TOPBP1 nucleolar localization and association with Treacle (Fig. 5 F) but, to a certain degree, decreased ATR activation and transcriptional repression in nucleoli (Fig. 5, H and I). In this regard, we can recall that BRCT7–8 can provide (i) the recognition and binding of TOPBP1 to ATR autophosphorylated at T1989 that stimulates further ATR kinase activity (Liu et al., 2011) or (ii) oligomerization of TOPBP1 (Liu et al., 2013). Together, these results suggest that the efficient silencing of nucleolar transcription not only depends on the physical interaction between TOPBP1 and Treacle but also requires substantial TOPBP1-mediated activation of ATR.

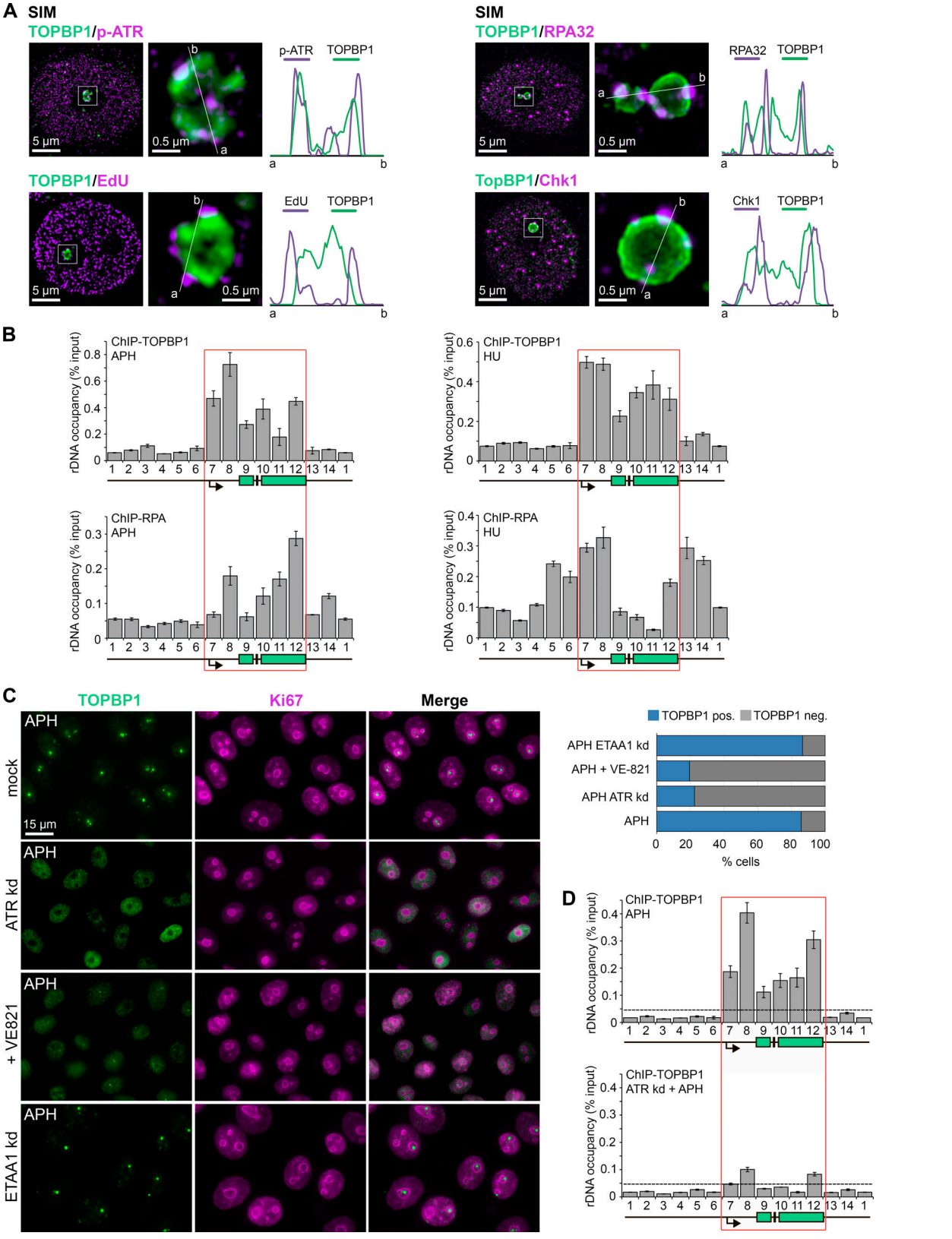

Figure 2. **Replication stress response in nucleoli. (A)** APH-treated (1 µM, 12 h) HeLa cells were stained for TOPBP1 (green) and either phospho-ATR (p-ATR; Thr1989), RPA32, CHK1, or EdU (magenta) that was incorporated and revealed as described in Fig. 1 A. SIM analyses were performed. Enlarged TOPBP1-containing FCs are shown in the insets. Colocalization analysis was performed. Graphs show quantification in arbitrary units of the distribution of TOPBP1 and corresponding replication stress protein fluorescence along the lines shown in the figures. **(B)** Occupancy of TOPBP1 and RPA at the rDNA of HeLa cells treated with APH (1 µM, 12 h) or HU (1 mM, 12 h). ChIP was followed by qPCR using the rDNA amplicons positioned as indicated on the scheme in Fig. 1 D. Data are

represented relative to the input. Values are mean ± SD from at least three independent replicates. 45S RNA coding regions on the histograms are marked by red squares. **(C)** Intact HeLa cells, ATR knockdown, VE-821 (an ATR inhibitor; 15 µM, 3 h), and ETAA1 knockdown HeLa cells were treated with APH (1 µM, 12 h) and immunostained against TOPBP1 (green) and nucleolar marker Ki67 (magenta). Percentage of cells containing large TOPBP1 foci is shown on the right. **(D)** Occupancy of TOPBP1 at the rDNA of APH-treated control and ATR knockdown (kd) HeLa cells. ChIP was performed as described in B. neg., negative; pos., positive.

TOPBP1 and Treacle prevent replication stress–induced nucleolar transcription silencing

The involvement of TOPBP1 and Treacle in the replication stress response in nucleoli made it reasonable to suggest that replication stress also repressed nucleolar transcription. Surprisingly, both an EU incorporation assay and RT-qPCR showed that neither APH nor HU treatment induced remarkable (and statistically significant) nucleolar transcription silencing (Fig. S4, A–D). SIM analyses of the EU-labeled newly synthesized RNA and FISH-labeled rRNA further showed that nucleolar transcription was unaltered under conditions of replication stress (Fig. S4, E and F). At the same time, a significant decrease of

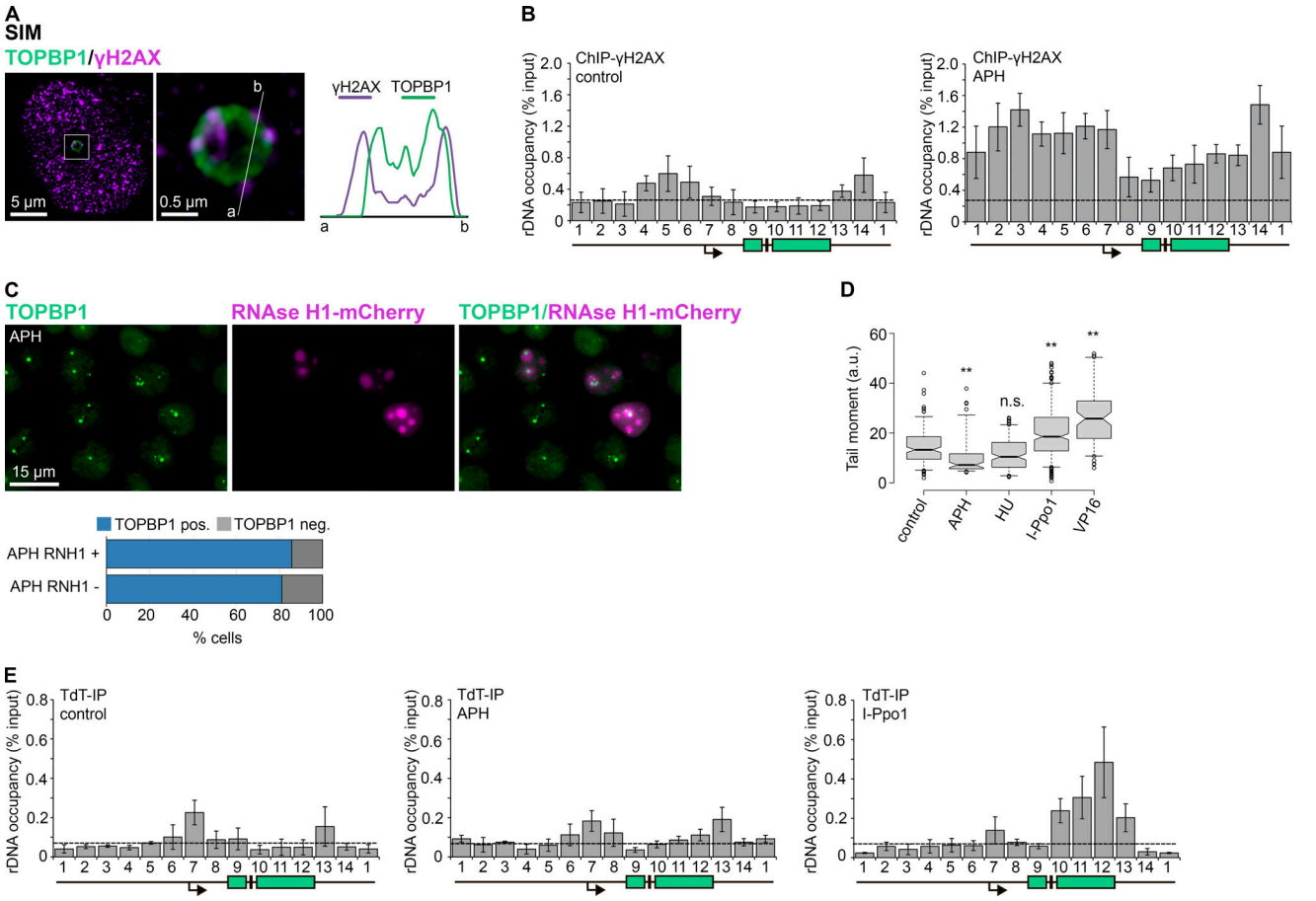

Figure 3. **Replication stress response in nucleoli does not depend on R loop stabilization or DSB generation. (A)** Representative SIM image of the HeLa cell treated with APH (1 µM, 12 h) and stained for TOPBP1 (green) and γH2AX (magenta). Enlarged TOPBP1-containing FCs are shown in the insets. Colocalization analysis was performed. Graphs show quantification in arbitrary units of the distribution of TOPBP1 and γH2AX fluorescence along the lines shown in the figures. **(B)** Occupancy of TOPBP1 and γH2AX at the rDNA of HeLa cells treated or not treated with APH (1 µM, 12 h). ChIP was followed by qPCR using the rDNA amplicons positioned as indicated on the scheme in Fig. 1 D. Data are represented relative to the input. Values are mean ± SD from at least three independent replicates. 45S RNA coding regions on the histograms are marked by green squares. **(C)** HeLa cells transiently overexpressing RNase H1-mCherry fusion protein (pICE-RNaseHI-WT-NLS-mCherry plasmid was a gift from Patrick Calsou, Addgene, Watertown, MA; Addgene plasmid #60365) were subjected to APH treatment (1 µM, 12 h), fixed, and immunostained for TOPBP1 (green). The percentage of cells with large TOPBP1 foci was quantified in the RNase H1-mCherry expressing ($RNH1^+$) and not expressing ($RNH1^-$) the cell population. **(D)** HeLa cells were treated with either APH (1 µM, 12 h), HU (1 mM, 12 h), or DNA topoisomerase II inhibitor etoposide (VP16; 10 µg/ml, 1 h). HeLa cells expressing homing endonuclease I-PpoI were treated with 4-hydroxytamoxifen for 4 h to activate I-PpoI. Control represents untreated HeLa cells. The neutral comet assay was performed; box plots show the tail moment. Horizontal lines represent the median. **, $P < 0.01$ by unpaired *t* test ($n > 2,000$). **(E)** DSB generation in rDNA was studied in control HeLa cells, HeLa cells treated with APH (1 µM, 12 h), and HeLa cells expressing I-PpoI and treated with 4-hydroxytamoxifen to activate it. DSB detection assay (TdT-IP) was followed by qPCR using the rDNA amplicons positioned as indicated on the scheme in Fig. 1 D. Data are represented relative to the input. Values are mean ± SD from at least three independent replicates. neg., negative; pos., positive.

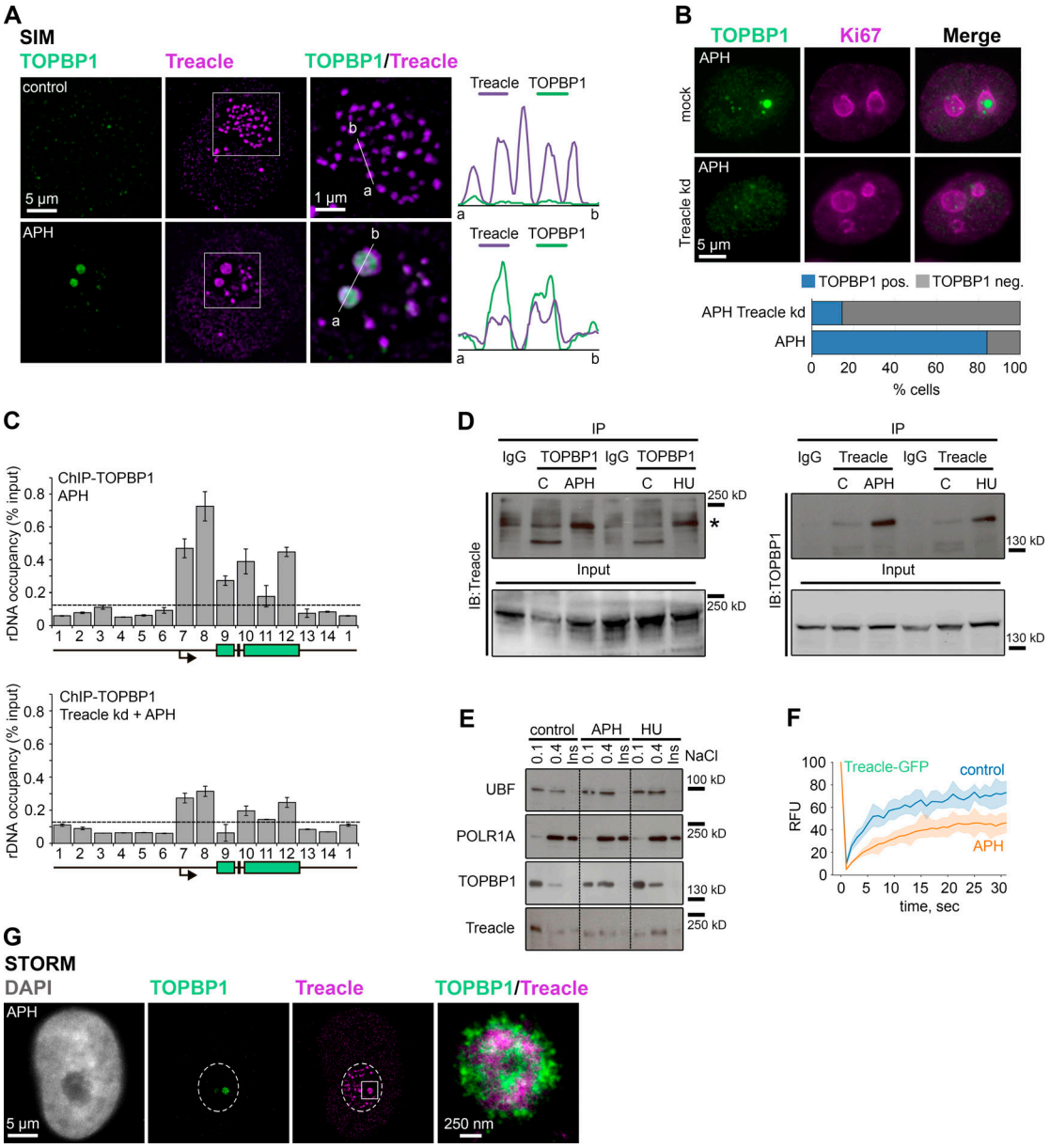

Figure 4. **Replication stress stimulates TOPBP1–Treacle interaction. (A)** Intact and APH-treated (1 µM, 12 h) HeLa cells were stained for TOPBP1 (green) and Treacle (magenta) and analyzed by SIM. Enlarged nucleoli are shown in the insets. Colocalization analysis was performed on the merged images. Graphs illustrate quantification in arbitrary units of the distribution of TOPBP1 and Treacle fluorescence along the lines shown in the figures. **(B)** Intact HeLa cells and Treacle knockdown (kd) HeLa cells were treated with APH (1 µM, 12 h) and immunostained against TOPBP1 (green) and nucleolar marker Ki67 (magenta). Percentage of cells containing large TOPBP1 foci is shown below. **(C)** Occupancy of TOPBP1 at the rDNA of APH-treated control and Treacle kd HeLa cells. ChIP was followed by qPCR using the rDNA amplicons positioned as indicated on the scheme in Fig. 1 D. Data are represented relative to the input. Values are mean ± SD from at least three independent replicates. **(D)** HeLa cells were untreated (C) or treated with either APH (1 µM, 12 h) or HU (1 mM, 12 h). TOPBP1 (left) or Treacle (right) were immunoprecipitated with an equal amount of the corresponding antibody or an unspecific IgG as a control. The immunoprecipitates were examined for the presence of Treacle (left) or TOPBP1 (right). An asterisk marks a true Treacle band. **(E)** Western blot analysis of UBF, Pol I (POLR1A), TOPBP1, and Treacle in different chromatin fractions from control and APH-treated (1 µM, 12 h) or HU-treated (1 mM, 12 h) HeLa cells prepared by sequential extraction with 0.1 and 0.4 M NaCl. **(F)** Kinetics of Treacle-GFP studied by FRAP in control and APH-treated (1 µM, 12 h) HeLa cells. The shaded parts of the lines represent SD. **(G)** Representative double-STORM image of TOPBP1 (green) and Treacle (magenta) in human HeLa cells that had been treated with APH (1 µM, 12 h), fixed, and immunostained for these factors. Nucleoli are marked by dashed lines. Replication stress–induced large TOPBP1-positive FC is shown in the right panel. IB, immunoblot; Ins, insoluble chromatin fraction; neg., negative; pos., positive; RFU, relative fluorescence unit.

nucleolar transcription was induced by replication stress in HeLa cells depleted for TOPBP1 or Treacle (Fig. 6 A). ChIP analysis with the anti–Pol I antibody additionally confirmed this observation; in cells depleted for TOPBP1 or Treacle, replication stress induced a reduction in the level of Pol I at the 45S coding region (Fig. 6 B). Bearing in mind that ATR was needed for the accumulation of TOPBP1 in nucleoli and its association with Treacle (Fig. 2, C and D; and Fig. 5), we additionally investigated

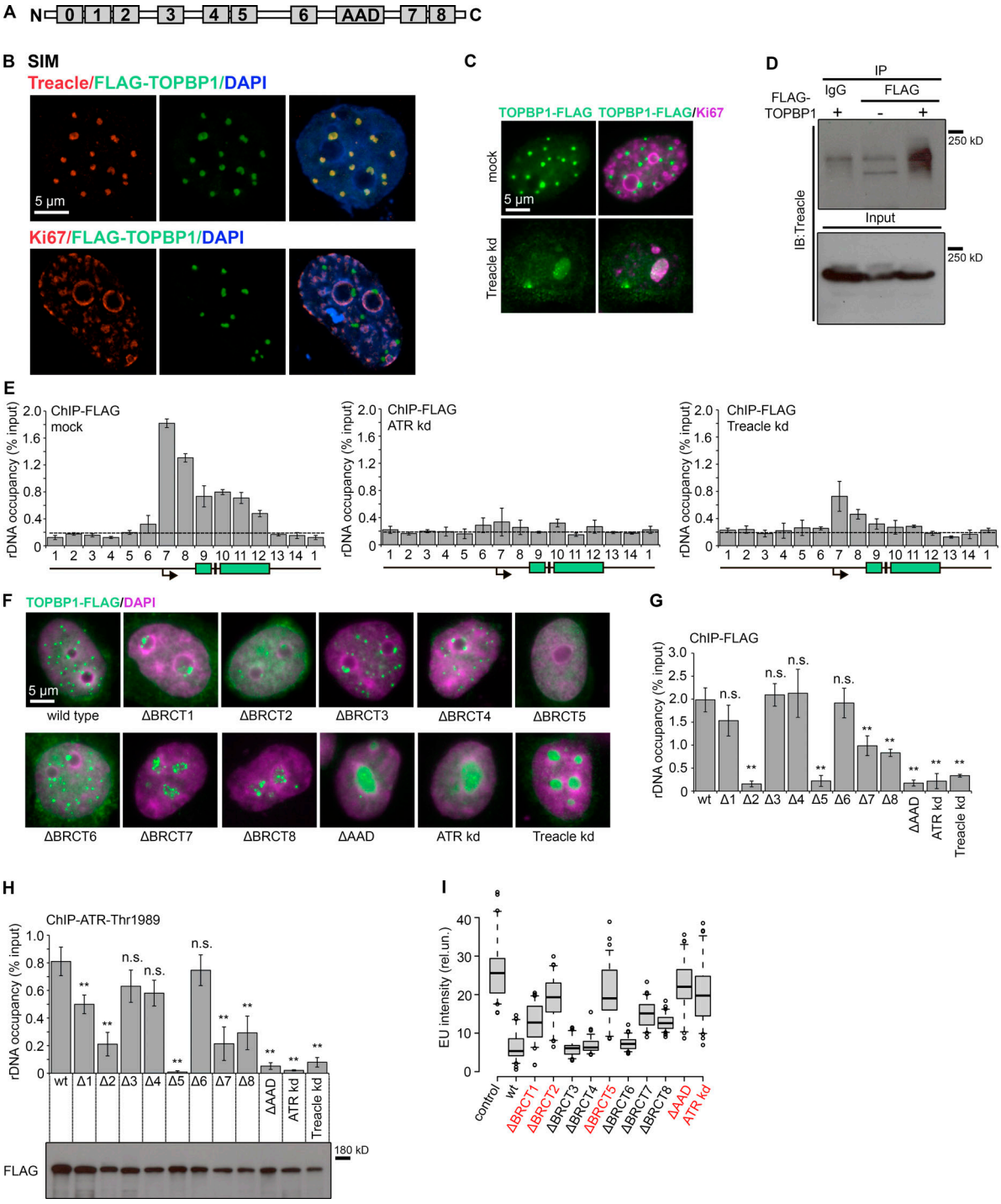

Figure 5. **Characterization of TOPBP1–Treacle interaction. (A)** Scheme of TOPBP1 domain structure. BRCT domains are depicted by the corresponding numbers. **(B)** SIM analysis of HeLa cells that were transiently transfected with TOPBP1-FLAG plasmid, fixed, and stained with antibodies against FLAG (green) and either Treacle or Ki67 (red). The DNA was stained with DAPI (blue). **(C)** Intact and Treacle knockdown (kd) HeLa cells were transfected with TOPBP1-FLAG plasmid, fixed, and stained with antibodies against FLAG (green) and Ki67 (magenta). **(D)** Cell extracts were prepared from HeLa cells not expressing (–) or expressing (+) FLAG-TOPBP1 protein. FLAG-fused TOPBP1 was immunoprecipitated with an equal amount of the anti-FLAG M2 antibody or an unspecific IgG as a control. The immunoprecipitates were examined for the presence of Treacle. **(E)** Occupancy of TOPBP1-FLAG protein at the rDNA of control HeLa cells or cells depleted for either ATR or Treacle. HeLa cells were transiently transfected with TOPBP1-FLAG plasmid and subjected to ChIP analysis. ChIP was performed using the antibody against FLAG followed by qPCR using the rDNA amplicons positioned as indicated on the scheme in Fig. 1 D. Data are represented relative to the input. Values are mean ± SD from at least three independent replicates. **(F)** HeLa cells depleted (knockout) for endogenous TOPBP1 were transfected with plasmid constructs encoding FLAG-fused full-length TOPBP1 or FLAG-fused TOPBP1 deletion mutants lacking AAD (ΔAAD) or individual BRCT domains (ΔBRCT1–8). Additionally, FLAG-fused full-length TOPBP1 was expressed and stained in HeLa cells depleted for either ATR or Treacle (kd). The cells were fixed and stained with antibodies against FLAG (green). The DNA was stained with DAPI (magenta). **(G and H)** Occupancy of FLAG-conjugated TOPBP1 deletion mutants (G) or phospho-ATR (Thr1989; H) at the rDNA of HeLa cells prepared as in F. ChIP was followed by qPCR using the rDNA #7 amplicon

positioned as indicated on the scheme in Fig. 1 D. Data are represented relative to the input. Values are mean ± SD from at least three independent replicates. **, P < 0.01 by unpaired *t* test. Below the histogram in H, Western blot analysis of FLAG-fused TOPBP1 variants in cells prepared as in F. **(I)** Quantification of EU fluorescence intensities in HeLa cells prepared as in F; control represents the cells depleted for endogenous TOPBP1. Horizontal lines represent the median. IB, immunoblot.

the nucleolar transcription in HeLa cells with genetically or pharmacologically downregulated ATR activity. As expected, the results were essentially the same as for the cells depleted of either TOPBP1 or Treacle (Fig. 6 A). These results suggest that in the case of nucleolar replication stress, transcriptional silencing originates from the accumulation of stalled replication forks, which represent a physical obstacle for Pol I. Therefore, TOPBP1 and Treacle are indispensable for providing efficient replication stress recovery and preventing stalled replication fork accumulation. ChIP analysis with the anti-RPA antibody supported this hypothesis: In HeLa cells depleted for TOPBP1, Treacle, or ATR, replication stress was exacerbated compared with APH-treated control cells (Fig. 6 C). Next, we performed a SIM-based colocalization analysis of FCs and replication stress foci that were marked with RPA (Fig. 6 D). Whereas in APH-treated HeLa cells only 20% of FCs colocalized with replication stress foci, in cells depleted for either TOPBP1 or Treacle and then treated with APH, replication stress was induced in almost all FCs (Fig. 6 D).

Finally, we performed anti-BrdU ChIP-qPCR analysis and found that the depletion of TOPBP1, Treacle, or ATR led to a complete inability of the replication machinery to resume DNA synthesis after removal of APH from the culture medium (Fig. 6 E). In summary, these results reveal that the Treacle–TOPBP1–ATR axis is indispensable for efficient and timely recovery from replication stress induced in nucleoli; the deficiency of these factors leads to nonregulated repression of nucleolar transcription.

TOPBP1 and Treacle facilitate recruitment of replication stress response factors inside the nucleoli

DSBs in rDNA stimulate FC aggregation at the nucleolar periphery in the form of nucleolar caps (Korsholm et al., 2019; Mooser et al., 2020). It is widely accepted that the formation of nucleolar caps (i) depends on transcription inhibition induced by DNA damage and (ii) enables the recruitment of repair factors normally excluded from nucleoli (van Sluis and McStay, 2019). Our study's results show that replication stress does not induce transcriptional repression and nucleolar cap formation. Large intranuclear Treacle–TOPBP1 foci seem to functionally substitute nucleolar caps and provide a molecular platform for cellular responses to replication stress. To study this process further, we performed super-resolution microscopy of two principal factors involved in the replication stress response—BRCA1 and FANCD2. These proteins easily entered nucleoli upon APH-induced replication stress and occupied the periphery of large TOPBP1-positive FCs (Fig. 7 A) in the same manner as RPA or ATR (see Fig. 2 A). Next, we analyzed whether the recruitment of these repair factors was dependent on Treacle or TOPBP1. The depletion of either Treacle or TOPBP1 significantly altered the recruitment of the repair factors inside the nucleoli upon 12 h of replication stress (Fig. 7 A). The ChIP-qPCR analysis also showed that BRCA1 and FANCD2 are efficiently recruited to the rDNA upon replication stress in a TOPBP1- and Treacle-dependent manner (Fig. 7 B). Taken together, these data show the importance of Treacle and its interacting partner TOPBP1 as a molecular platform providing recruitment of stress response factors inside the nucleoli under DNA replication stress. However, this dependency on Treacle and TOPBP1 was characteristic for the initial 12–16 h of replication stress; further exacerbation of replication stress led to Treacle- and TOPBP1-independent recruitment of BRCA1 and FANCD2. This was evidenced by time-resolved ChIP-qPCR analyses of BRCA1 and FANCD2 in control and Treacle-depleted cells treated with APH for up to 24 h (Fig. 7 C) and by SIM analyses of BRCA1 and FANCD2 in Treacle- or TOPBP1-depleted cells exposed to replication stress for 20 h (Fig. S5 A).

TOPBP1 and Treacle maintain genome stability during nucleolar replication stress

We next aimed to establish the biological significance of the TOPBP1–Treacle association in nucleoli. We hypothesized that replication stress–induced formation of large TOPBP1 foci in nucleoli is necessary for the reinforcement of ATR activation and, thus, the prevention of excessive origin firing that might otherwise be induced by replication stress. Indeed, ChIP-qPCR analysis showed that ATR and its target kinase CHK1 were recruited and activated at the rDNA in response to replication stress (Fig. 8 A). In cells depleted for either TOPBP1 or Treacle, such activation was completely abrogated (Fig. 8 A). As a consequence, dormant replication origins will fire followed by the accumulation of stalled replication forks, since this is happening under conditions of APH or HU treatment. Our experimental data—specifically, SIM analyses of RPA, BRCA1, and FANCD2 (Fig. 6 D and Fig. S5 A)—corroborate this idea.

Our data show that in general, rDNA/nucleolus is barely susceptible to replication stress; it requires prolonged incubation with replication stress triggers like APH or HU to induce nucleolar replication stress. Even when replication stress in rDNA is induced, it lacks immediate serious consequences, such as replication fork collapse (Fig. 6 E) and generation of DSBs (Fig. 3, D and E). To check whether nucleolar replication stress had delayed consequences, we treated the cells with APH for 12 h, released them in fresh culture medium, and followed them for up to 24 h. By using a DSB detection assay and ChIP-qPCR, we investigated DSB generation and ATM activation during different recovery periods (3, 6, 12, and 24 h) after replication stress (Fig. 8 B). While in control HeLa cells APH did not stimulate delayed DSB formation and ATM activation, HeLa cells depleted for either Treacle, TOPBP1, or ATR reacted differently (Fig. 8 B). Specifically, we found that a deficiency in the Treacle–TOPBP1–ATR axis led to the accumulation of DSBs and

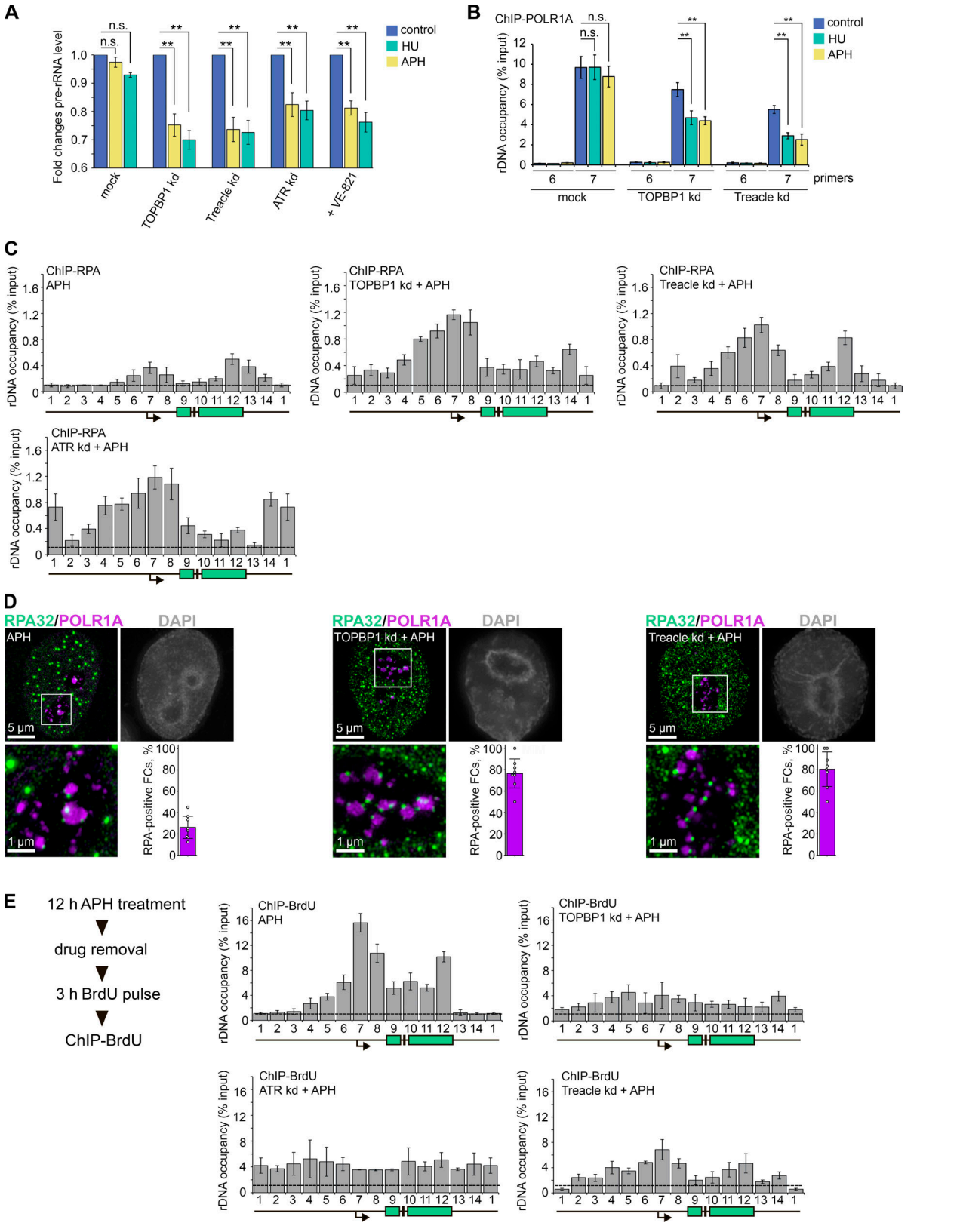

Figure 6. **TOPBP1 and Treacle prevent replication stress–induced silencing of nucleolar transcription. (A)** Intact (mock-treated) HeLa cells; HeLa cells depleted for either TOPBP1, Treacle, or ATR; and HeLa cells incubated with an ATR inhibitor VE-821 (15 µM, 3 h) were not treated (control) or treated with either APH (1 µM, 12 h) or HU (1 mM, 12 h). qRT-PCR was performed. Levels of pre-rRNA normalized to GAPDH mRNA are shown. Values are mean ± SD. **, P < 0.01 by unpaired *t* test. **(B)** Occupancy of Pol I (POLR1A) at the rDNA of HeLa cells depleted for TOPBP1 or Treacle and then treated with either APH or HU as described in A. ChIP was followed by qPCR using rDNA #6 and #7 amplicons positioned as indicated on the scheme in Fig. 1 D. Data are represented relative to

the input. Values are mean ± SD from at least three independent replicates. **P < 0.01 by unpaired *t* test. **(C)** Occupancy of RPA32 at the rDNA of APH-treated (1 µM, 12 h) HeLa cells or cells first depleted for either TOPBP1, Treacle, or ATR and then treated with APH. ChIP was followed by qPCR using the rDNA amplicons positioned as indicated on the scheme in Fig. 1 D. Data are represented relative to the input. Values are mean ± SD from at least three independent replicates. **(D)** APH-treated (1 µM, 12 h) HeLa cells or cells first depleted for either TOPBP1 or Treacle and then treated with APH were immunostained for RPA32 (green) and Pol I (POLR1A; magenta) and analyzed by SIM. The DNA was stained with DAPI (gray). Enlarged nucleoli are shown in the insets. Percentage of FCs (marked by POLR1A) containing RPA foci is shown in each case. **(E)** Control HeLa cells and HeLa cells depleted for either TOPBP1, Treacle, or ATR were cultured with APH (1 µM, 12 h) and then were pulse labeled with BrdU (100 µM, 3 h) in fresh medium. BrdU incorporation across rDNA was analyzed by the BrdU-IP assay. It was followed by qPCR using the rDNA amplicons positioned as indicated on the scheme in Fig. 1 D. Data are represented relative to the input. Values are mean ± SD from at least three independent replicates. kd, knockdown.

corresponding activation of ATM in rDNA by the 24-h recovery time point (Fig. 8 B). Together, these data show the importance of Treacle and its interacting partner TOPBP1 as a molecular platform providing recruitment of stress response factors inside the nucleoli and reinforcing ATR activation under DNA replication stress, thus limiting genome instability.

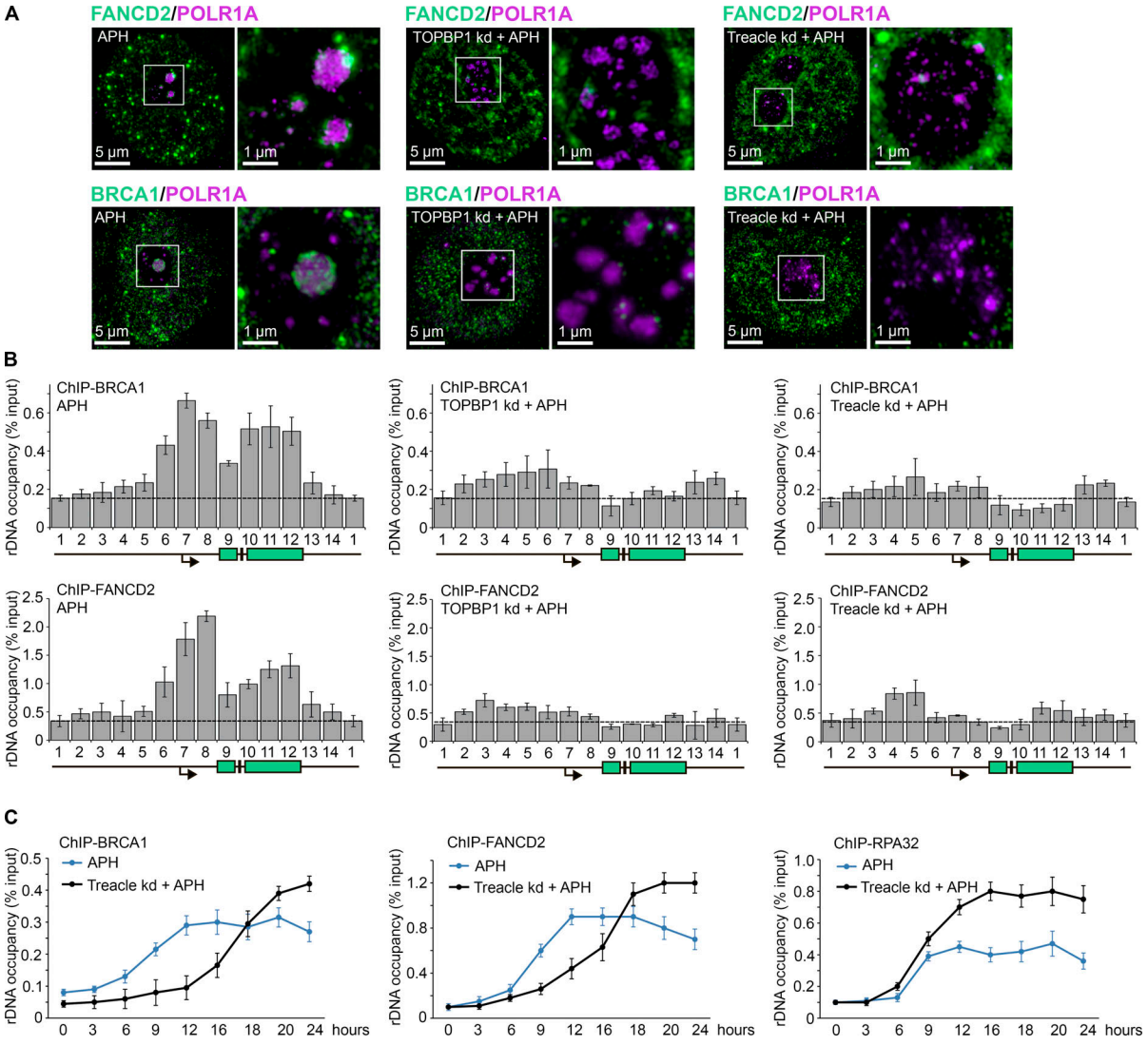

Figure 7. **TOPBP1 and Treacle facilitate recruitment of replication stress response factors inside nucleoli. (A)** APH-treated (1 µM, 12 h) HeLa cells or cells first depleted for either TOPBP1 or Treacle and then treated with APH were immunostained for Pol I (POLR1A; magenta) and either FANCD2 or BRCA1 (green). Samples were analyzed with SIM. Enlarged nucleoli are shown in the insets. **(B)** Occupancy of replication stress response factors at the rDNA of APH-treated (1 µM, 12 h) HeLa cells or cells first depleted for either TOPBP1 or Treacle and then treated with APH. ChIP with antibodies against BRCA1 and FANCD2 followed by qPCR using the rDNA amplicons positioned as indicated on the scheme in Fig. 1 D. Data are represented relative to the input. Values are mean ± SD from at least three independent replicates. **(C)** Control (mock-treated) HeLa cells and HeLa cells depleted for Treacle were cultured with APH (1 µM) for different periods (0, 3, 6, 9, 12, 20, or 24 h). ChIP with antibodies against BRCA1, FANCD2, and RPA32 followed by qPCR using rDNA #7 amplicons positioned as indicated on the scheme in Fig. 1 D. Data are represented relative to the input. Values are mean ± SD from three independent replicates. kd, knockdown.

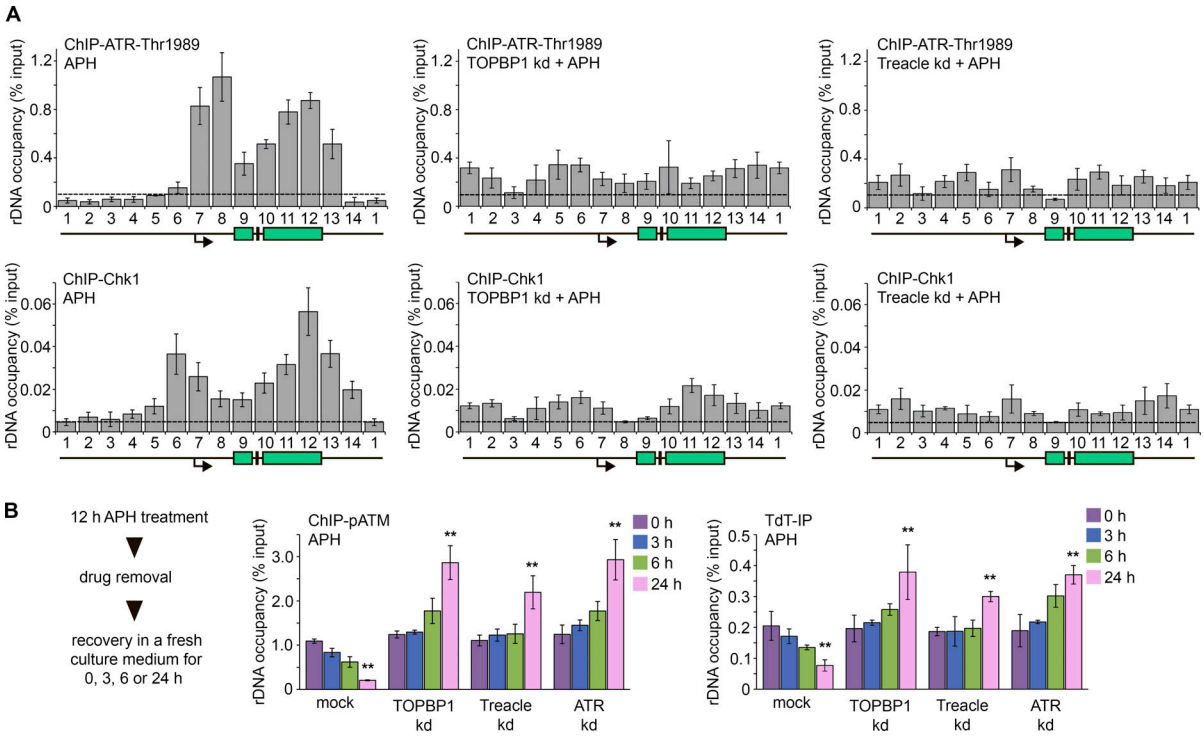

Figure 8. **TOPBP1 and Treacle maintain genome stability during nucleolar replication stress. (A)** Occupancy of phospho-ATR (Thr1989) and CHK1 at the rDNA of APH-treated (1 µM, 12 h) HeLa cells or cells first depleted for either TOPBP1 or Treacle and then treated with APH. ChIP was followed by qPCR using the rDNA amplicons positioned as indicated on the scheme in Fig. 1D. Data are represented relative to the input. Values are mean ± SD from at least three independent replicates. **(B)** Control (mock-treated) HeLa cells and HeLa cells depleted for either TOPBP1, Treacle, or ATR were cultured with APH (1 µM, 12 h) and then incubated in a fresh medium for different periods (0, 3, 6, or 24 h). ChIP with anti–phospho-ATM antibody and DSB detection assay (TdT-IP) were followed by qPCR using rDNA #7 amplicons positioned as indicated on the scheme in Fig. 1 D. Data are represented relative to the input. Values are mean ± SD from at least three independent replicates. **, $P < 0.01$ by unpaired *t* test. kd, knockdown.

Discussion

rDNA repeats are some of the most actively transcribed regions in the genome. Consequently, the precise spatiotemporal control of DNA replication and transcription of rDNA repeats is indispensable for maintaining the genome stability of rDNA arrays. To avoid head-to-head collisions of replication machinery with elongating Pol I, replication forks move codirectionally with the transcription along the 45S coding region (Dimitrova, 2011; Lebofsky and Bensimon, 2005). Replication forks moving in an opposing direction are stopped by a replication fork barrier located just downstream of the 45S RNA coding region (Akamatsu and Kobayashi, 2015; Dimitrova, 2011). However, replication fork stalling at rDNA is still possible in normal conditions and even more so under replication stress conditions. To the best of our knowledge, the present study is the first to investigate the molecular outcomes of the replication stress induced in rDNA of the higher eukaryotes. We demonstrate that in response to drug-induced replication stress, initial DDR factors such as RPA, TOPBP1, and ATR are recruited inside the nucleolus. The BRCA1- and FANCD2-dependent pathways are also activated. It is noteworthy that all these factors are recruited at the FCs located inside the nucleoli. Thus, it is not mandatory to extrude FCs that contain stalled replication forks to the nucleolar periphery and form nucleolar caps to attract DDR factors or amplify DDR signaling as in the case of rDNA DSBs (Larsen and Stucki, 2016). Our results also suggest that the hypothetic incompatibility of DDR factors with nucleolar liquid phases (van Sluis and McStay, 2019) is not a cause for nucleolar cap formation.

It is well known that lesions in rDNA provoke regulated repression of Pol I–dependent transcription (van Sluis and McStay, 2019). We did not manage to show that replication stress could induce regulated massive silencing of nucleolar transcription. It seems that the transcription is transiently stopped only at sites of replication fork stalling; hence, it is difficult to detect a statistically significant decrease in the transcriptional level. However, this situation changes substantially when replication stress is induced in cells depleted for TOPBP1 or Treacle that makes the cells incapable to activate an ATR-dependent checkpoint pathway. In these cells, the inability to recover in a timely manner replication forks stalled at rDNA repeats and excessive origin firing leads to progressive accumulation of FCs containing stalled replication forks and, in turn, results in significant transcriptional repression.

One of the most intriguing features of the nucleolar replication stress response is its total dependency on TOPBP1–Treacle interaction. The necessity for TOPBP1–Treacle interaction for correct nucleoli-specific DDR was reported recently by our group and the group of Manuel Stucki (Mooser et al., 2020; Velichko et al., 2019). Here, we also demonstrate that such interaction is indispensable during nucleolar replication stress.

Treacle and TOPBP1 facilitate ATR signaling at stalled replication forks in the nucleolus and reinforce ATR-mediated checkpoint activation to limit genome instability. Characterization of the Treacle–TOPBP1 interaction mode allows us to propose that these factors can form a molecular platform for efficient stress response in the nucleolus. Using GFP-fused TOPBP1 and its deletion mutants, we confirmed that the interaction between TOPBP1 and Treacle is constitutive and DNA damage independent. We also demonstrate that BRCT1-2, BRCT5, and AAD of the TOPBP1 are indispensable for its interaction with Treacle, ATR activation, and repression of nucleolar transcription. Moreover, we show, for the first time, that TOPBP1 BRCT7 and 8 contribute to these processes as well. It is therefore likely that for efficient ATR activation and transcriptional silencing, TOPBP1 should not only interact with Treacle but also undergo BRCT7–8–dependent oligomerization, forming a molecular platform for DDR factor recruitment. Decreased mobility of Treacle and TOPBP1 proteins residing in nucleoli under replication stress conditions support this idea.

Nucleolar phosphoprotein Treacle, the product of the TCOF1 gene, is drawing ever-increasing attention. Its direct role in Pol I–dependent transcription is not clear (Lin and Yeh, 2009). Furthermore, an increasing number of studies have reported the role of Treacle in recruitment and/or retention of different nonnucleolar proteins in nucleoli (Fages et al., 2020; Kong et al., 2019; Larsen et al., 2014; Mooser et al., 2020; Rawlinson et al., 2018; Velichko et al., 2019). It is clear that Treacle can interact with BRCT-containing factors (Larsen et al., 2014; Mooser et al., 2020; Velichko et al., 2019); however, it is not known whether Nbs1 and TOPBP1 are the only BRCT proteins that interact with Treacle. It might be that such an enigmatic role of Treacle in some of the nucleolar processes strongly depends on its nature. According to various predictors of protein complexity (e.g., PONDR and IUPred2A), Treacle is one of the most intrinsically disordered proteins, which hypothetically makes it potent for modulating nucleolar liquid phases.

Materials and methods

Cell culture and drug treatment

Human HeLa cells (CCL-2™; ATCC), U2OS (HTB-96™; ATCC), MCF7 (HTB-22™; ATCC), HeLa Kyoto (kindly provided by A.S.M.), HCT116 and HCT116 with p53 knockout (kindly provided by Prof. Boris Zhivotovsky, Karolinska Institut, Stockholm, Sweden), human skin fibroblasts (female 46XX), and mouse CT26 (CRL-2638™; ATCC) were cultured in DMEM (PanEco) supplemented with 10% FBS (HyClone; GE Healthcare) and penicillin/streptomycin. The cells were cultured at 37°C in a conventional humidified CO_2 incubator. Replication stress was induced by the treatment of cells with 1 mM HU (Sigma-Aldrich) or 1 μM APH (Sigma-Aldrich) for 12 h.

Gene knockdown

RNA interference experiments were performed using DharmaFECT siRNA transfection reagent (Thermo Fisher Scientific) following the manufacturer's instructions. The cells were transfected with 50 nM ATR siRNA (#sc-29763; Santa Cruz Biotechnology), 50 nM Treacle/TCOF1 (#sc-61707; Santa Cruz Biotechnology), 50 nM TOPBP1 (#sc-41068; Santa Cruz Biotechnology), and 50 nM ETAA1 (#sc-94927; Santa Cruz Biotechnology). The TOPBP1 knockout HeLa cell line was established earlier (Velichko et al., 2019). Briefly, for CRISPR/Cas9-mediated knockout, two single-guide RNAs (sgRNAs) flanking a region of the TOPBP1 gene were designed using the ATUM gRNA Design Tool (gRNA1: 5′-CACCGAAACTGGATGTTCGGCTCTT-3′ (forward), 5′-AAACAAGAGCCGAACATCCAGTTTC-3′ (reverse); gRNA2: 5′-CACCGATATATCTTTGCGGTTTTAG-3′ (forward), 5′-AAACCTAAAACCGCAAAGATATATC-3′ (reverse). The sgRNA-targeting sequences were separately cloned into the sgRNA/Cas9 expression vector pSpCas9n(BB)-2A-Puro (PX462) V2.0 (#62987; Addgene). The plasmids were cotransfected into HeLa cells with Xfect transfection reagent (Clontech Laboratories). The transfectants were selected with 10 μg/ml puromycin for 24 h. After 24 h of puromycin selection, cells were switched to their normal culture medium. Clones of HeLa cells were obtained by limiting dilution into 96-well plates. Knockdown/knockout efficiency was analyzed by Western blotting (Fig. S5 B).

Chromatin-enriching salt separation and immunoblotting

HeLa cells were incubated in a lysis buffer (LB; 10 mM Hepes-NaOH, pH 7.5, 1.5 mM $MgCl_2$, 0.5 mM EDTA, 10 mM KCl, 0.5% NP-40, phosphatase, and protease inhibitors). Cells were incubated at 4°C for 10 min and collected by centrifugation at 1,000 x*g* for 5 min. Cells were then incubated in an LB containing 100 mM NaCl. After incubation at 4°C for 10 min, the first soluble fraction ("0.1" fraction) was separated by centrifugation at 10,000 x*g* for 10 min. Cells were then incubated in an LB containing 400 mM NaCl. After incubation at 4°C for 1 h, the second soluble fraction ("0.4" fraction) was separated from the chromatin fraction by centrifugation at 8,000 x*g* for 10 min. The chromatin pellet ("insoluble" fraction) was then sonicated in an LB at 1/2 amplitude for 30 s with a VirSonic 100 ultrasonic cell disrupter.

Aliquots of each sample were separated by SDS-PAGE and blotted onto polyvinylidene fluoride membranes. The membranes were blocked for 1 h in 2% ECL Advance Blocking Reagent (GE Healthcare) or 2% BSA (Sigma-Aldrich) in PBS containing 0.1% Tween 20 (PBS-T) followed by incubation overnight at 4°C with primary antibodies diluted in PBS-T containing 2% blocking reagent or 2% BSA. After three washes with PBS-T, the membranes were incubated for 1 h with secondary antibodies (HRP-conjugated anti-rabbit or anti-mouse IgG) in PBS-T containing 2% blocking agent or 2% BSA. The immunoblots were visualized using a Pierce ECL Plus Western blotting substrate. Antibodies used in the study are listed in Table S1.

Gene expression analysis

RNA was extracted from cells using TRIzol reagent (Life Technologies). All RNA samples were further treated with DNase I (Thermo Fisher Scientific) to remove the residual DNA. RNA (1 μg) was reverse transcribed in a total volume of 20 μl for 1 h at 42°C using 0.4 μg of random hexamer primers and 200 U of reverse transcription (Thermo Fisher Scientific) in the presence

of 20 U ribonuclease inhibitor (Thermo Fisher Scientific). The cDNA obtained was analyzed by qPCR using the CFX96 Touch Real-Time PCR detection system (Bio-Rad Laboratories). The PCRs were performed in 20-µl reaction volumes that included 50 mM Tris-HCl (pH 8.6), 50 mM KCl, 1.5 mM $MgCl_2$, 0.1% Tween 20, 0.5 µM of each primer, 0.2 mM of each deoxynucleoside triphosphate, 0.6 µM EvaGreen (Biotium), 0.2 U Hot Start Taq Polymerase (SibEnzyme), and 50 ng cDNA. Primers used in the study are listed in Table S2. Levels of pre-rRNA normalized to GAPDH mRNA are shown in the corresponding figures.

Fluorescence microscopy (including super-resolution microscopy)

For immunostaining, cells were grown on microscope slides. All samples were fixed in CSK buffer (10 mM Pipes, pH 7.0, 100 mM NaCl, 1.5 mM $MgCl_2$, 300 mM sucrose) supplemented with 1% PFA and 2.5% Triton X-100 for 15 min at room temperature. Cells were washed in PBS and then incubated with antibodies in PBS supplemented with 1% BSA and 0.05% Tween 20 for 1 h at room temperature or overnight at 4°C. The cells were then washed three times (5 min each time) with PBS. The primary antibodies bound to antigens were visualized using Alexa Fluor 488–conjugated secondary antibodies. The DNA was counterstained with the fluorescent dye DAPI for 10 min at room temperature. The samples were mounted using Dako Fluorescent Mounting Medium (Life Technologies). The immunostained samples were analyzed using a Zeiss Axio Scope.A1 fluorescence microscope (Zeiss N-Achroplan 40×/0.65 NA and EC Plan-Neofluar 100×/1.3 NA oil objectives, Zeiss AxioCam MRm camera, Zeiss AxioVision release 4.8.2 acquisition software) or a Leica STELLARIS 5 confocal microscope (HC PL APO 63×/1.40 NA oil CS2 objective). The images were processed using ImageJ software (version 1.44). The images were analyzed using CellProfiler software (version 3.1.5).

Samples for SIM were mounted in Dako Fluorescence Mounting Medium (Life Technologies) and examined using a Nikon N-SIM microscope (100×/1.49 NA oil immersion objective, 488- and 561-nm diode laser excitation). Image stacks (z-steps of 120 nm) were acquired with an electron-multiplying charge-coupled devices camera (Andor iXon 897; effective pixel size, 60 nm). Exposure conditions were adjusted to get a typical yield of ∼5,000 maximum counts (16-bit raw image) while keeping bleaching minimal. Image acquisition, SIM image reconstruction, and data alignment were performed using NIS-Elements (Nikon). 3D reconstruction of x, y, z SIM datasets (z-stacks) was performed using Imaris 7.4 (Bitplane).

For STORM, cells were grown on 35-mm imaging dishes (Ibidi). All samples were fixed in CSK buffer (10 mM Pipes, pH 7.0, 100 mM NaCl, 1.5 mM $MgCl_2$, 300 mM sucrose) supplemented with 1% PFA and 2.5% Triton X-100 for 15 min at room temperature. After washing once with 1× PBS, the cells were incubated with TOPBP1 and Treacle antibodies diluted in blocking buffer (1% BSA in 1× PBS with 0.05% Tween 20) at 4°C overnight. The cells were washed three times with 1× PBS for 5 min per wash, and the Alexa Fluor 647– and Atto 488–conjugated secondary antibodies in the blocking buffer were added to the sample for 1 h. The cells were washed three times with 1× PBS and stored in 1× PBS before imaging. Immediately before imaging, PBS was replaced with STORM imaging buffer containing 10% (wt/vol) glucose (Sigma-Aldrich), 50 mM Tris-HCl (pH 8.0), 10 mM NaCl, 0.56 mg/ml glucose oxidase (Sigma-Aldrich), 0.17 mg/ml catalase (Sigma-Aldrich), and 0.14 M β-mercaptoethanol (Sigma-Aldrich). All imaging experiments were performed using a commercial ONI Nanoimager microscope system (Oxford Nanoimaging). The emitted light was collected by an oil immersion 100×/1.49 NA objective and imaged onto a scientific CMOS camera. For STORM imaging, 50,000 frames were acquired at an exposure time of 10 ms. The reconstruction of the super-resolution image was performed using NimOS software (Oxford Nanoimaging). Antibodies used in the study are listed in Table S1.

FRAP analysis

Two days prior to imaging, cells were transiently transfected with plasmid encoding GFP-Treacle (a gift from Rita Shiang, Addgene, Watertown, MA; Addgene plasmid #74300; Winokur and Shiang, 1998). FRAP experiments were performed on the Nikon Ti-E microscope with Plan Apo oil objective (60×/1.4 NA) and Nikon C2+ camera at 37°C in a humidified incubator. For bleaching and imaging of eGFP-Treacle, a 488-nm laser was used. After bleaching, cells were imaged every 5 s for 30 s. Resulting images were analyzed using ImageJ software (version 1.44).

ChIP

Cells were fixed for 15 min with 1% formaldehyde at room temperature, and crosslinking was quenched by adding 125 mM glycine for 5 min. Cells were harvested in PBS, and nuclei were prepared by incubation in FL buffer (5 mM Pipes, pH 8.0, 85 mM KCl, 0.5% NP-40) supplemented with Protease Inhibitor Cocktail (Bimake) and Phosphatase Inhibitor Cocktail (Bimake) for 30 min on ice. Next, chromatin was sonicated in radioimmunoprecipitation assay buffer (10 mM Tris-HCl, pH 8.0, 140 mM NaCl, 1% Triton X-100, 0.1% Na-deoxycholate, 0.1% SDS) with a VirSonic 100 to an average length of 200–500 bp. Per ChIP reaction, ∼10–20 µg chromatin was incubated with 2–4 µg antibodies overnight at 4°C. The next day, Protein A/G Magnetic Beads (Thermo Fisher Scientific) were added to each sample and incubated for 4 h at 4°C. Immobilized complexes were washed two times for 10 min at 4°C in low-salt buffer (20 mM Tris-HCl, pH 8.0, 150 mM NaCl, 2 mM EDTA, 0.1% SDS, 1% Triton X-100) and high-salt buffer (20 mM Tris-HCl, pH 8.0, 500 mM NaCl, 2 mM EDTA, 0.1% SDS, 1% Triton X-100). Samples were incubated with RNase A (Thermo Fisher Scientific) for 30 min at room temperature. The DNA was eluted from the beads and decrosslinked by proteinase K digestion for 4 h at 55°C and subsequent incubation at 65°C for 12 h. Next, the DNA was purified using phenol/chloroform extraction and analyzed by qPCR. The qPCR primers used for ChIP analysis are listed in Table S3. Data in the corresponding figures are represented relative to the input. Values are the mean ± SD from at least three independent replicates.

BrdU-IP

HeLa cells were cultured for 12 h in a medium containing 1 µM APH (Sigma-Aldrich). After that, nascent DNA was pulse labeled by incubating the cells in fresh medium supplemented with 100 µM 5-BrdU (Sigma-Aldrich) for 2 h. Cellular DNA was isolated, sonicated to ∼500-bp fragments, and heat denatured; 2 µg of genomic DNA was incubated at 4°C overnight with 1.5 µg of anti-BrdU antibodies in 150 mM NaCl, 10 mM phosphate buffer (pH 7.2), and 0.05% Triton X-100. On the next day, Protein A/G Magnetic Beads (Thermo Fisher Scientific) were added to each sample and incubated for 4 h at 4°C. Immobilized DNA–antibody complexes were washed two times for 10 min at 4°C in a low-salt buffer (20 mM Tris-HCl, pH 8.0, 150 mM NaCl, 2 mM EDTA, 0.1% SDS, 1% Triton X-100) and high-salt buffer (20 mM Tris-HCl, pH 8.0, 500 mM NaCl, 2 mM EDTA, 0.1% SDS, 1% Triton X-100). Proteins were digested for 4 h at 55°C with proteinase K, and DNA was purified by phenol/chloroform extractions and ethanol precipitation.

Replication and transcription labeling

For EdU incorporation, cells were incubated with 10 µM EdU (Life Technologies) for 0.5–1 h at 37°C. Then, the cells were washed three times with PBS and fixed in CSK buffer (10 mM Pipes, pH 7.0, 100 mM NaCl, 1.5 mM $MgCl_2$, 300 mM sucrose) supplemented with 1% PFA and 2.5% Triton X-100 for 15 min at room temperature. The samples were then processed using a Click-iT EdU Imaging Kit (Life Technologies) according to the manufacturer's recommendations.

For EU incorporation, the cells were incubated with 200 µM EU (Sigma-Aldrich) for 30 min at 37°C. Then, the cells were washed three times with PBS and fixed in CSK buffer (10 mM Pipes, pH 7.0, 100 mM NaCl, 1.5 mM $MgCl_2$, 300 mM sucrose) supplemented with 1% PFA and 2.5% Triton X-100 for 15 min at room temperature. The samples were then processed using a Click-iT EU Imaging Kit (Life Technologies) according to the manufacturer's recommendations.

Protein coimmunoprecipitation

Cell extracts were prepared in the following IP buffer for 30 min on ice: 50 mM Tris (pH 7.5), 120 mM NaCl, 10% glycerol, 0.5% NP-40, and 1 mM EDTA supplemented with Protease Inhibitor Cocktail (Bimake), Phosphatase Inhibitor Cocktail (Bimake), and 25 U/ml benzonase (Sigma-Aldrich). Lysates were cleared by centrifugation at 14,000 x*g* for 15 min and incubated with anti-Flag M2 (#F3165; Sigma-Aldrich), anti-TOPBP1 (mouse, #sc-271043; Santa Cruz Biotechnology), or anti-Treacle (rabbit, #HPA038237; Sigma-Aldrich) antibodies for 4 h at 4°C. Next, protein A/G Magnetic Beads (Thermo Fisher Scientific) were added to each sample and incubated for another 4 h. Mouse IgG (#015-000-002; Jackson ImmunoResearch) or rabbit IgG (#011-000-002; Jackson ImmunoResearch) was used as a negative control. Ig–antigen complexes were washed three times with IP buffer before elution in the SDS sample buffer.

Neutral comet assay

After the treatments, cells were trypsinized with 0.25% trypsin for several minutes at 37°C. Trypsin was inactivated with a fourfold volume of DMEM. Cell suspension at a concentration of 10^5 cells/ml was mixed in a 1:1 ratio with LMAgarose (#4250-050-02; Trevigen) at 37°C. The mixture was pipetted onto Comet slides (#3950-300-02; Trevigen) that had been precoated with a 1% normal-melting-point agarose (Sigma-Aldrich) base layer. The drop containing the cells was covered with a glass coverslip and incubated at 4°C for 5 min. After the incubation, the coverslips were removed, and the slides were immersed in lysis solution (30 mM EDTA, 0.5% SDS, and 10 mM Tris-HCl, pH 8.0, supplemented with 500 µg/ml proteinase K) and incubated at 37°C for 1 h. After lysis, the slides were washed three times for 5 min in PBS and incubated in 1× Tris-borate-EDTA buffer for 20 min at 4°C. Electrophoresis was performed in a Trevigen electrophoresis system (#4250-050-ES) for 10 min at 4°C and 1 V/cm in 1× Tris-borate-EDTA buffer. The comets were counterstained with SYBR Green for 1 h (1:3,000, #S7563; Thermo Fisher Scientific). The comets were visualized using an inverted Nikon Eclipse Ti-E fluorescence microscope equipped with a Nikon Intensilight C-HGFI light source (Nikon Plan Fluor 4×/0.13 NA objective, DS-Qi2 camera). The images of the comets were analyzed using CellProfiler software (version 2.1.1, revision 6c2d896).

Single-molecule RNA FISH

All single-molecule RNA FISH probes were designed as previously described (Yao et al., 2019) and labeled with Cy3 on the 3′ ends (Table S4). Cells were fixed with 4% PFA for 15 min followed by permeabilization with 1% Triton X-100 for 10 min. Cells were incubated in 10% formamide/2× SSC for 10 min at room temperature and then hybridized with 5 nM each of the RNA probes in 50% formamide/2× SSC at 37°C for 16 h. After hybridization, the cells were washed with 10% formamide/2× SSC for 30 min at 37°C and incubated with antibodies as described above to visualize proteins.

rDNA FISH

Cells were fixed with 1% formaldehyde in 1× PBS for 15 min and then washed three times with 1× PBS and permeabilized with 0.5% Triton X-100 for 30 min. After permeabilization, cells were washed three times with 1× PBS. Next, cells were treated with 10 µg/ml RNase A in 2× SSC at 37°C for at least 45 min, followed by denaturation with 0.1 N HCl at room temperature for 15 min. Cells were then washed two times with 2× SSC and incubated in 50% formamide in 2× SSC for at least 30 min at room temperature. Fluorescein-labeled probes for human rDNA (bacterial artificial chromosome clone RP11-450E20) were obtained from Empire Genomics. Cover glasses with cells were denaturated with rDNA probe in hybridization buffer (2 µl probe and 8 µl hybridization buffer per cover glass) at 84°C for 7 min and hybridized at 37°C for 24 h. After hybridization, cells were washed three times (5 min each) with 50% formamide in 2× SSC at 45°C and then twice with 1× SSC at 45°C and once with 1× SSC at room temperature. Finally, cells were washed with ultrapure water (Milli-Q) and stained with DAPI or proceeded to immunofluorescence staining of proteins.

DNA DSB detection assay

Cells were fixed with Streck Tissue Fixative (0.15 M 2-bromo-2-nitropropane-1,3-diol, 0.1 M diazolidinyl urea, 0.04 M zinc

sulfate heptahydrate, 0.01 M sodium citrate dihydrate, 50 mM EDTA) at room temperature for 20 min. The cells were washed with cold PBS twice and subsequently resuspended in Buffer A (0.25% Triton X-100, 10 mM EDTA, 10 mM Hepes, pH 6.5) and Buffer B (200 mM NaCl, 1 mM EDTA, 10 mM Hepes, pH 6.5). After permeabilization of the nuclei with Buffer C (100 mM Tris-HCl, pH 7.4, 50 mM EDTA, 1% Triton X-100) for 30 min at 4°C, the nuclei were sequentially washed with cold PBS, deionized water, and 1× TdT reaction buffer (Thermo Fisher Scientific). Cells were subsequently incubated in 1 ml reaction buffer (1× TdT buffer, 0.005% Triton X-100, 45 µM biotin-14-dATP [Jena Bioscience], and 250 U TdT) for 90 min at 37°C. Cells were washed twice with ice-cold TBS (50 mM Tris-HCl, pH 7.5, 150 mM NaCl) and then lysed in 200 µl LB (50 mM Tris-HCl, pH 8.0, 10 mM EDTA, 1% SDS) for 15 min at 37°C. Chromatin was sheared using a VirSonic 100 sonicator into ∼500-bp fragments and diluted. Biotinylated DNA fragments were captured with 50 µl of Dynabeads MyOne Streptavidin C1 magnetic beads (Invitrogen) for 4 h at room temperature. Beads were washed three times in 450 µl radioimmunoprecipitation assay ChIP buffer and twice in 200 µl TE buffer. DNA was analyzed by qPCR. The qPCR primers used for ChIP analysis are listed in Table S3.

Statistical analysis

ChIP and RT-PCR data are reported as mean values from at least three biological replicates, with error bars denoting the SD. Immunostaining and comet assay images were analyzed by CellProfiler software; the measurements obtained are presented in box-and-whisker plots. At least 500 cells were analyzed in each experiment. Comparisons between two groups were performed using a paired two-tailed Student's *t* test using IBM SPSS Statistics version 20 software.

Online supplemental material

Fig. S1 expands the data on replication stress–induced accumulation of TOPBP1 in nucleoli. Fig. S2 shows that nucleolar TOPBP1 foci are formed due to replication stress but not to accumulation of the cells in S phase. Fig. S3 shows which of the TOPBP1 domains are crucial for repression of nucleolar transcription. Fig. S4 shows that replication stress does not induce repression of nucleolar transcription. Fig. S5 shows that Treacle or TOPBP1 depletion exacerbates replication stress and presents gene knockdown and knockout efficiencies. Table S1 is a complete list of antibodies used in the study. Tables S2 lists oligonucleotides used in RT-qPCR experiments. Table S3 lists oligonucleotides used in ChIP-qPCR experiments. Table S4 lists oligonucleotides used in RNA FISH experiments.

Acknowledgments

We thank Prof. Jiadong Wang (Peking University Health Science Center, Beijing, China) for the gift of FLAG-fused TOPBP1 deletion mutants. SIM and FRAP experiments were performed using the equipment purchased within the framework of the Lomonosov Moscow State University development program. This work was performed using the equipment of the Center for Precision Genome Editing and Genetic Technologies for Biomedicine, Institute of Gene Biology Russian Academy of Sciences. The ChIP and FISH experiments performed during the revision of the paper were supported by the Russian Science Foundation (21-64-00001).

The authors declare no competing financial interests.

Author contributions: Conceptualization, A.K. Velichko, O.L. Kantidze, S.V. Razin; methodology, A.K. Velichko; investigation, A.K. Velichko, N.V. Petrova, A.V. Luzhin, M. Panyavina; investigation–SIM, A.K. Velichko, N. Ovsyannikova, I.I. Kireev; investigation–STORM, A.K. Velichko, A.S. Gavrikov, A.S. Mishin; supervision, A.K. Velichko, O.L. Kantidze; writing–original draft, O.L. Kantidze; writing–review and editing, A.K. Velichko, O.L. Kantidze, S.V. Razin.

Submitted: 16 August 2020
Revised: 26 April 2021
Accepted: 18 May 2021

References

Akamatsu, Y., and T. Kobayashi. 2015. The human RNA polymerase I transcription terminator complex acts as a replication fork barrier that coordinates the progress of replication with rRNA transcription activity. *Mol. Cell. Biol.* 35:1871–1881. https://doi.org/10.1128/MCB.01521-14

Andersen, J.S., Y.W. Lam, A.K. Leung, S.E. Ong, C.E. Lyon, A.I. Lamond, and M. Mann. 2005. Nucleolar proteome dynamics. *Nature.* 433:77–83. https://doi.org/10.1038/nature03207

Berti, M., D. Cortez, and M. Lopes. 2020. The plasticity of DNA replication forks in response to clinically relevant genotoxic stress. *Nat. Rev. Mol. Cell Biol.* 21:633–651. https://doi.org/10.1038/s41580-020-0257-5

Blackford, A.N., and S.P. Jackson. 2017. ATM, ATR, and DNA-PK: The Trinity at the Heart of the DNA Damage Response. *Molecular Cell.* 66:801–817. https://doi.org/10.1016/j.molcel.2017.05.015

Cerqueira, A.V., and B. Lemos. 2019. Ribosomal DNA and the nucleolus as keystones of nuclear architecture, organization, and function. *Trends Genet.* 35:710–723. https://doi.org/10.1016/j.tig.2019.07.011

Couté, Y., J.A. Burgess, J.J. Diaz, C. Chichester, F. Lisacek, A. Greco, and J.C. Sanchez. 2006. Deciphering the human nucleolar proteome. *Mass Spectrom. Rev.* 25:215–234. https://doi.org/10.1002/mas.20067

Dimitrova, D.S. 2011. DNA replication initiation patterns and spatial dynamics of the human ribosomal RNA gene loci. *J. Cell Sci.* 124:2743–2752. https://doi.org/10.1242/jcs.082230

Fages, J., C. Chailleux, J. Humbert, S.M. Jang, J. Loehr, J.P. Lambert, J. Côté, D. Trouche, and Y. Canitrot. 2020. JMJD6 participates in the maintenance of ribosomal DNA integrity in response to DNA damage. *PLoS Genet.* 16:e1008511. https://doi.org/10.1371/journal.pgen.1008511

Feric, M., N. Vaidya, T.S. Harmon, D.M. Mitrea, L. Zhu, T.M. Richardson, R.W. Kriwacki, R.V. Pappu, and C.P. Brangwynne. 2016. Coexisting liquid phases underlie nucleolar subcompartments. *Cell.* 165:1686–1697. https://doi.org/10.1016/j.cell.2016.04.047

Frattini, C., A. Promonet, E. Alghoul, S. Vidal-Eychenie, M. Lamarque, M.P. Blanchard, S. Urbach, J. Basbous, and A. Constantinou. 2021. TopBP1 assembles nuclear condensates to switch on ATR signaling. *Mol. Cell.* 81:1231–1245.e8. https://doi.org/10.1016/j.molcel.2020.12.049

Ju, B.G., V.V. Lunyak, V. Perissi, I. Garcia-Bassets, D.W. Rose, C.K. Glass, and M.G. Rosenfeld. 2006. A topoisomerase IIbeta-mediated dsDNA break required for regulated transcription. *Science.* 312:1798–1802. https://doi.org/10.1126/science.1127196

Kong, X., Y.-Y. Chen, J. Lin, E. Flowers, E. Van Nostrand, S.M. Blue, J. Chau, C.I.-H. Ma, I. Mohr, R. Thai, et al. 2019. The cohesin loader NIPBL interacts with pre-ribosomal RNA and treacle to regulate ribosomal RNA synthesis. *bioRxiv.* (Preprint posted June 4, 2019). https://doi.org/10.1101/658492

Korsholm, L.M., Z. Gál, L. Lin, O. Quevedo, D.A. Ahmad, E. Dulina, Y. Luo, J. Bartek, and D.H. Larsen. 2019. Double-strand breaks in ribosomal RNA genes activate a distinct signaling and chromatin response to facilitate nucleolar restructuring and repair. *Nucleic Acids Res.* 47:8019–8035. https://doi.org/10.1093/nar/gkz518

Larsen, D.H., and M. Stucki. 2016. Nucleolar responses to DNA double-strand breaks. *Nucleic Acids Res.* 44:538–544. https://doi.org/10.1093/nar/gkv1312

Larsen, D.H., F. Hari, J.A. Clapperton, M. Gwerder, K. Gutsche, M. Altmeyer, S. Jungmichel, L.I. Toledo, D. Fink, M.B. Rask, et al. 2014. The NBS1-Treacle complex controls ribosomal RNA transcription in response to DNA damage. *Nat. Cell Biol.* 16:792–803. https://doi.org/10.1038/ncb3007

Lebofsky, R., and A. Bensimon. 2005. DNA replication origin plasticity and perturbed fork progression in human inverted repeats. *Mol. Cell. Biol.* 25:6789–6797. https://doi.org/10.1128/MCB.25.15.6789-6797.2005

Lee, Y.C., Q. Zhou, J. Chen, and J. Yuan. 2016. RPA-binding protein ETAA1 is an ATR activator involved in DNA Replication stress response. *Curr. Biol.* 26:3257–3268. https://doi.org/10.1016/j.cub.2016.10.030

Lin, C.I., and N.H. Yeh. 2009. Treacle recruits RNA polymerase I complex to the nucleolus that is independent of UBF. *Biochem. Biophys. Res. Commun.* 386:396–401. https://doi.org/10.1016/j.bbrc.2009.06.050

Liu, S., B. Shiotani, M. Lahiri, A. Maréchal, A. Tse, C.C. Leung, J.N. Glover, X.H. Yang, and L. Zou. 2011. ATR autophosphorylation as a molecular switch for checkpoint activation. *Mol. Cell.* 43:192–202. https://doi.org/10.1016/j.molcel.2011.06.019

Liu, K., J.D. Graves, J.D. Scott, R. Li, and W.C. Lin. 2013. Akt switches TopBP1 function from checkpoint activation to transcriptional regulation through phosphoserine binding-mediated oligomerization. *Mol. Cell. Biol.* 33:4685–4700. https://doi.org/10.1128/MCB.00373-13

Mooser, C., I.E. Symeonidou, P.A. Leimbacher, A. Ribeiro, A.K. Shorrocks, S. Jungmichel, S.C. Larsen, K. Knechtle, A. Jasrotia, D. Zurbriggen, et al. 2020. Treacle controls the nucleolar response to rDNA breaks via TOPBP1 recruitment and ATR activation. *Nat. Commun.* 11:123. https://doi.org/10.1038/s41467-019-13981-x

Rawlinson, S.M., T. Zhao, A.M. Rozario, C.L. Rootes, P.J. McMillan, A.W. Purcell, A. Woon, G.A. Marsh, K.G. Lieu, L.F. Wang, et al. 2018. Viral regulation of host cell biology by hijacking of the nucleolar DNA-damage response. *Nat. Commun.* 9:3057. https://doi.org/10.1038/s41467-018-05354-7

Ray, S., T. Panova, G. Miller, A. Volkov, A.C. Porter, J. Russell, K.I. Panov, and J.C. Zomerdijk. 2013. Topoisomerase IIα promotes activation of RNA polymerase I transcription by facilitating pre-initiation complex formation. *Nat. Commun.* 4:1598. https://doi.org/10.1038/ncomms2599

Sokka, M., K. Rilla, I. Miinalainen, H. Pospiech, and J.E. Syväoja. 2015. High levels of TopBP1 induce ATR-dependent shut-down of rRNA transcription and nucleolar segregation. *Nucleic Acids Res.* 43:4975–4989. https://doi.org/10.1093/nar/gkv371

van Sluis, M., and B. McStay. 2019. Nucleolar DNA double-strand break responses underpinning rDNA genomic stability. *Trends Genet.* 35:743–753. https://doi.org/10.1016/j.tig.2019.07.001

Velichko, A.K., N.V. Petrova, A.V. Luzhin, O.S. Strelkova, N. Ovsyannikova, I.I. Kireev, N.V. Petrova, S.V. Razin, and O.L. Kantidze. 2019. Hypoosmotic stress induces R loop formation in nucleoli and ATR/ATM-dependent silencing of nucleolar transcription. *Nucleic Acids Res.* 47:6811–6825. https://doi.org/10.1093/nar/gkz436

Velichko, A.K., N.V. Petrova, S.V. Razin, and O.L. Kantidze. 2015. Mechanism of heat stress-induced cellular senescence elucidates the exclusive vulnerability of early S-phase cells to mild genotoxic stress. *Nucleic Acids Res.* 43:6309–6320.

Wang, J., Z. Gong, and J. Chen. 2011. MDC1 collaborates with TopBP1 in DNA replication checkpoint control. *J. Cell Biol.* 193:267–273. https://doi.org/10.1083/jcb.201010026

Wardlaw, C.P., A.M. Carr, and A.W. Oliver. 2014. TopBP1: a BRCT-scaffold protein functioning in multiple cellular pathways. *DNA Repair (Amst.).* 22:165–174. https://doi.org/10.1016/j.dnarep.2014.06.004

Winokur, S.T., and R. Shiang. 1998. The Treacher Collins syndrome (TCOF1) gene product, treacle, is targeted to the nucleolus by signals in its C-terminus. *Hum. Mol. Genet.* 7:1947–1952. https://doi.org/10.1093/hmg/7.12.1947

Yao, R.W., G. Xu, Y. Wang, L. Shan, P.F. Luan, Y. Wang, M. Wu, L.Z. Yang, Y.H. Xing, L. Yang, and L.L. Chen. 2019. Nascent pre-rRNA sorting via phase separation drives the assembly of dense fibrillar components in the human nucleolus. *Mol. Cell.* 76:767–783.e11. https://doi.org/10.1016/j.molcel.2019.08.014

Zou, L. 2017. DNA replication checkpoint: new ATR activator identified. *Curr. Biol.* 27:R33–R35. https://doi.org/10.1016/j.cub.2016.11.025

Supplemental material

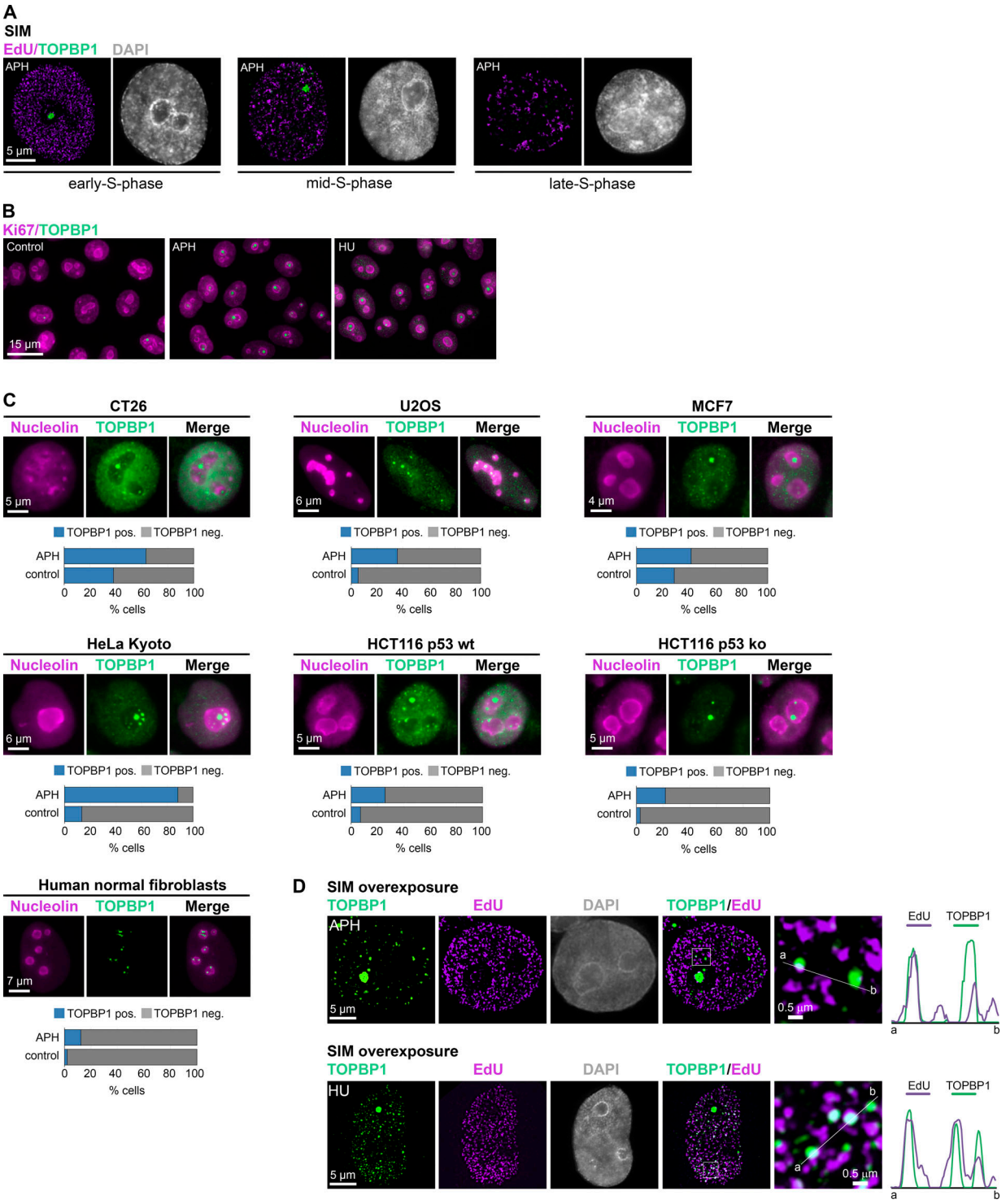

Figure S1. **Replication stress induces the accumulation of TOPBP1 in nucleoli. (A)** Representative SIM images of HeLa cells that were pulse labeled with EdU (10 µM, 30 min) and immunostained for TOPBP1 (green). EdU (magenta) was revealed by click chemistry. The DNA was stained with DAPI (gray). The cells were assigned to early, mid, or late S phases according to their EdU pattern (Velichko et al., 2015). **(B)** Control HeLa cells and cells treated with APH (1 µM, 12 h) or HU (1 mM, 12 h) were immunostained for TOPBP1 (green) and nucleolar marker Ki67 (magenta). **(C)** Different mouse (CT26) and human cell lines (U2OS, MCF7, HeLa Kyoto, and p53 WT and p53 knockout [ko] HCT116) and normal human fibroblasts were treated with APH (1 µM, 12 h) and immunostained for TOPBP1 (green) and nucleolin (magenta). Control represents untreated cells. Representative images are shown in each case. Percentage of cells containing large TOPBP1 foci is shown below the corresponding images. **(D)** SIM analysis of the HeLa cells that were pulse labeled with EdU (10 µM, 30 min) and immunostained for TOPBP1 (green). EdU (magenta) was revealed by click chemistry. The DNA was stained with DAPI (gray). Representative overexposed images are shown to demonstrate TOPBP1 staining in nucleoplasm along with large nucleolar TOPBP1 foci. Enlarged regions of nucleoplasm are shown in the insets. Colocalization analysis was performed. Graphs show quantification in arbitrary units of the distribution of TOPBP1 and EdU fluorescence along the lines shown in the figures. neg., negative; pos., positive.

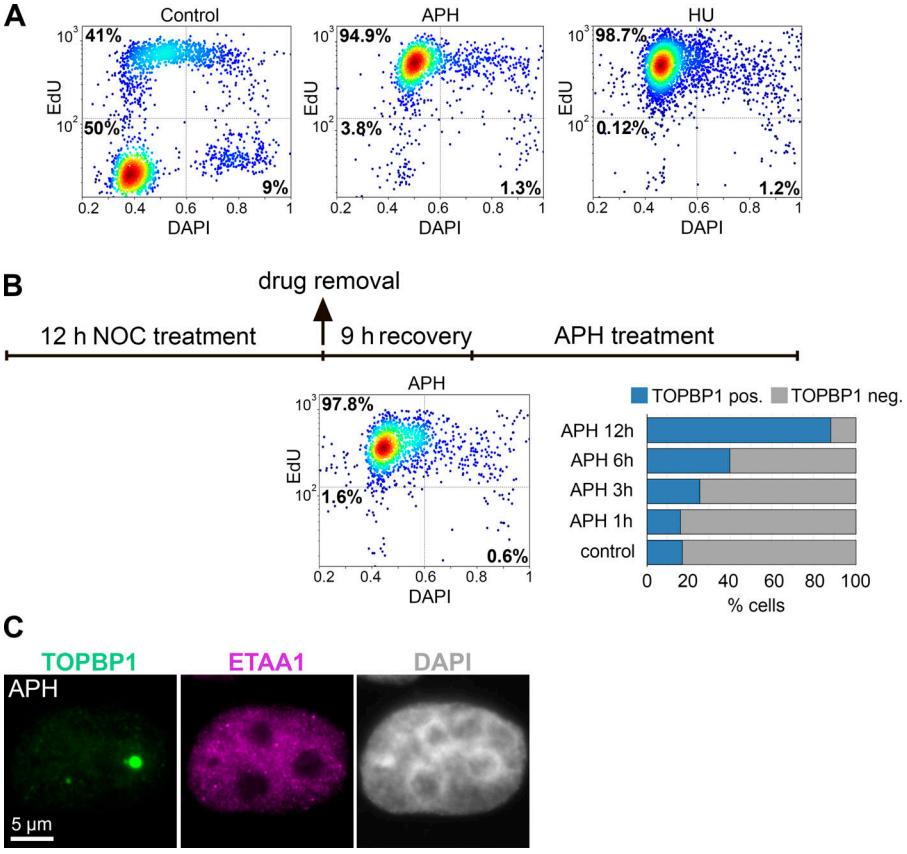

Figure S2. **Accumulation of the cells in the S-phase is not sufficient for large nucleolar TOPBP1 foci formation. (A)** Image-based analysis of cell-cycle distribution of control HeLa cells and cells treated with APH (1 µM, 12 h) or HU (1 mM, 12 h). **(B)** HeLa cells were synchronized in the S phase by treatment with nocodazole (NOC) for 12 h, incubation in fresh medium for an additional 9 h, and then treatment with APH (1 µM) for different periods (1, 3, 6, and 12 h). Synchronization accuracy was monitored using image-based analysis of cell-cycle distribution shown in the middle. Control represents the cells that were NOC synchronized in the S phase but not treated with APH. The cells were immunostained for TOPBP1. Percentage of cells containing large TOPBP1 foci is shown. **(C)** Representative image of HeLa cells that were treated with APH (1 µM, 12 h) and immunostained for TOPBP1 (green) and ETAA1 (magenta). The DNA was stained with DAPI (gray). neg., negative; pos., positive.

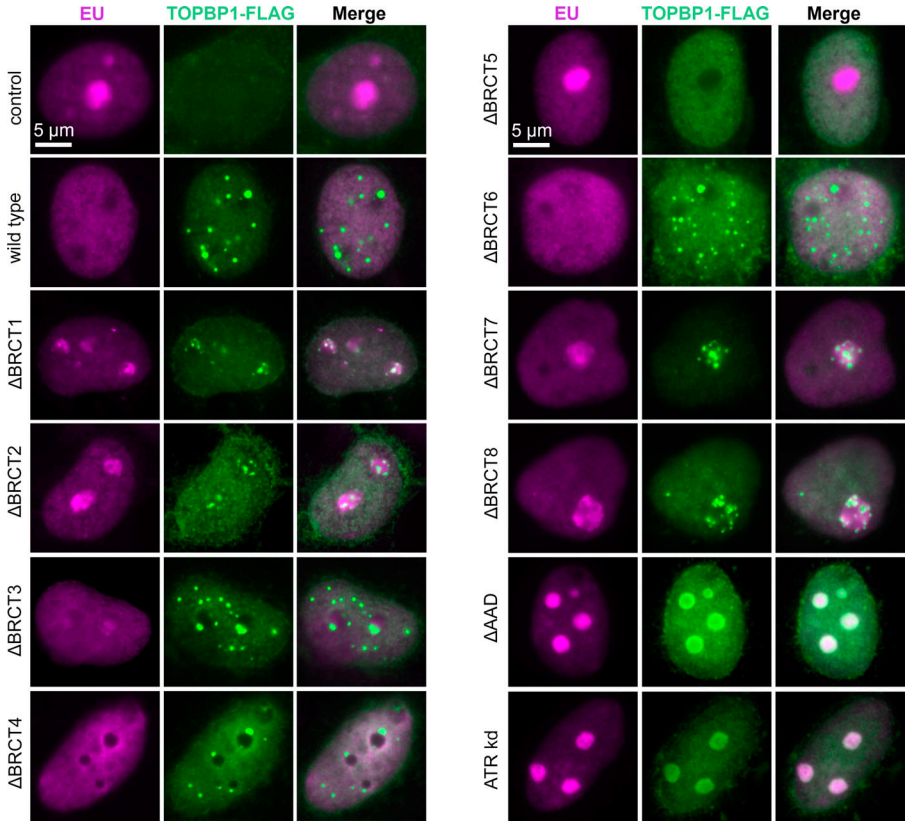

Figure S3. **Characterization of TOPBP1–Treacle interaction.** HeLa cells depleted for endogenous TOPBP1 were transfected with plasmid constructs encoding FLAG-fused full-length TOPBP1 or FLAG-fused TOPBP1 deletion mutants lacking AAD (ΔAAD) or individual BRCT domains (ΔBRCT1–8). Additionally, FLAG-fused full-length TOPBP1 was expressed and stained in HeLa cells depleted for ATR (knockdown [kd]). The cells were then pulsed with the EU (200 μM, 30 min). The cells were fixed and stained with antibodies against FLAG (green). EU (magenta) was revealed by click chemistry.

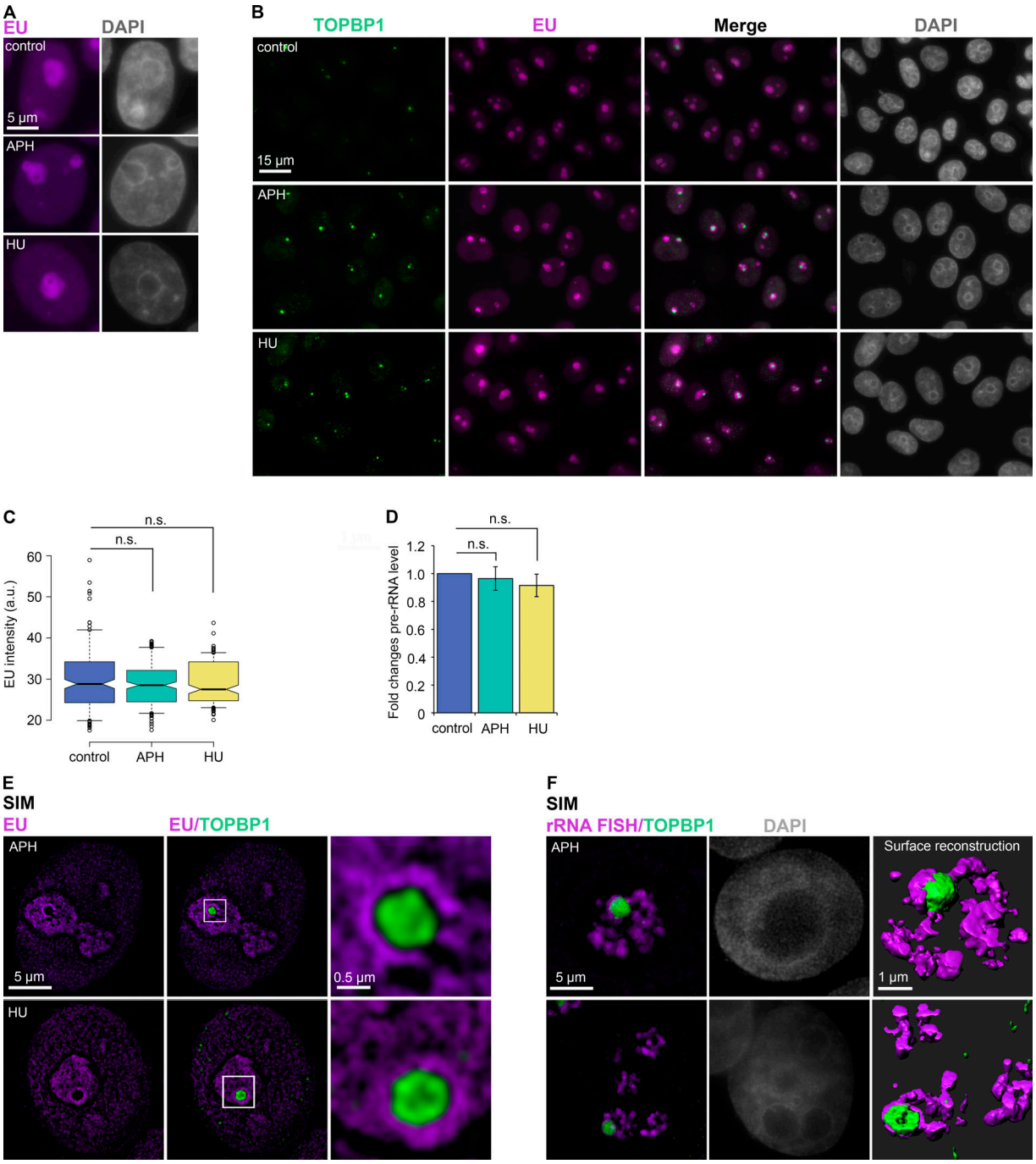

Figure S4. **Replication stress does not repress nucleolar transcription. (A)** HeLa cells, untreated or treated with APH (1 µM, 12 h) or HU (1 mM, 12 h), were pulsed with EU (1 mM, 30 min). EU (magenta) was revealed by click chemistry. The DNA was stained with DAPI (gray). Representative images are shown. **(B)** HeLa cells treated as in A were pulse labeled with EU, fixed, and immunostained for TOPBP1 (green). EU (magenta) was revealed by click chemistry. The DNA was stained with DAPI (gray). **(C)** Quantification of EU fluorescence intensities in HeLa cells treated as in A. Horizontal lines represent the median. Significance by unpaired *t* test ($n > 500$). **(D)** RT-qPCR showing levels of pre-rRNA normalized to GAPDH mRNA in HeLa cells treated as in A. Values are mean ± SD. Significance by unpaired *t* test ($n > 500$). **(E)** Representative SIM images of Hela cells treated and stained as in B. Enlarged nucleolar TOPBP1 foci are shown in the left panel. **(F)** Representative SIM images of HeLa cells treated with APH (1 µM, 12 h) or HU (1 mM, 12 h) and stained for TOPBP1 and rRNA (revealed by single-molecule FISH). Surface reconstructions of large nucleolar TOPBP1 foci and surrounding rRNA are shown in the left panel.

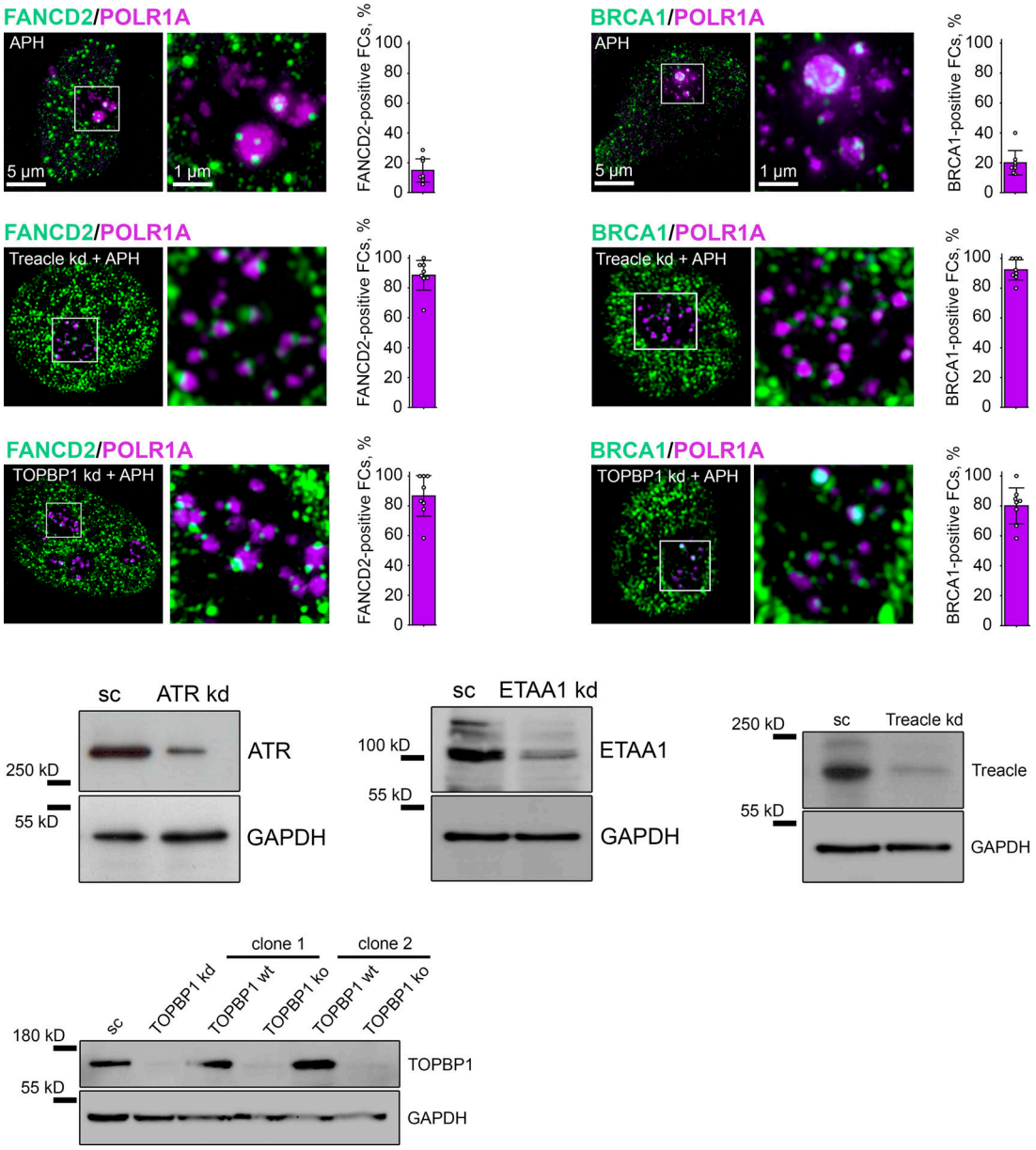

Figure S5. **Recruitment of BRCA1 and FANCD2 into the nucleolus in response to replication stress.** APH-treated (1 µM, 20 h) HeLa cells or cells first depleted for either TOPBP1 or Treacle and then treated with APH were immunostained for Pol I (POLR1A; magenta) and either FANCD2 or BRCA1 (green). Samples were analyzed with SIM. Enlarged nucleoli are shown in the insets. Percentage of FCs (marked by POLR1A) containing FANCD2 or BRCA1 foci are shown in each case. HeLa cells were depleted for either ATR, ETAA1, TOPBP1, or Treacle using RNA interference or CRISPR/Cas9 technology. Knockdown (kd) and knockout (ko) efficiencies were analyzed by Western blotting. sc, scrambled control.

Four tables are provided online as separate Word files. Table S1 is a complete list of antibodies used in the study. Tables S2 lists oligonucleotides used in RT-qPCR experiments. Table S3 lists oligonucleotides used in ChIP-qPCR experiments. Table S4 lists oligonucleotides used in RNA FISH experiments.